Towards Multiphase Simulations of Launch Environments for Acoustic Predictions

Jordan Angel
Michael Barad
Man Long Wong
Scott Neuhoff
Cetin Kiris

Computational Aerosciences Branch
NASA Ames Research Center

Advanced Modeling & Simulation (AMS) Seminar Series
NASA Ames Research Center, March 24, 2022

ARTEMIS I

https://appel.nasa.gov/wp-content/uploads/2020/11/artemis-1-update.jpg

The first uncrewed, integrated flight test of NASA's Orion spacecraft and Space Launch System rocket, launching from a modernized Kennedy spaceport

1 LAUNCH
SLS and Orion lift off from pad 39B at Kennedy Space Center

2 JETTISON ROCKET BOOSTERS
Solid rocket boosters separate

3 JETTISON LAUNCH ABORT SYSTEM (LAS)
The LAS is no longer needed, Orion could safely abort

4 CORE STAGE MAIN ENGINE CUT OFF (MECO) and separation

5 ENTER EARTH ORBIT
Perform the perigee raise maneuver

6 EARTH ORBIT
Systems check and solar panel adjustments

7 TRANS LUNAR INJECTION (TLI) BURN
Burn lasts for approximately 20 minutes

8 INTERIM CRYOGENIC PROPULSION STAGE (ICPS) SEPARATION
The ICPS has committed Orion to TLI

9 OUTBOUND TRANSIT
Requires several attitude maneuvers

10 OUTBOUND TRAJECTORY CORRECTION (OTC) BURNS
As necessary adjust trajectory for Lunar flyby to DRO

11 OUTBOUND POWERED FLYBY (OPF)
62 miles from the Moon; targets DRO insertion

Heliocentric Disposal precludes re-contact

12 ORBIT INSERTION
Enter Distant Retrograde Orbit for next 6-23 days

13 DISTANT RETROGRADE ORBIT (DRO)
Orbit Maintenance burns and solar panel adjustments; 38,000 nmi from the surface of the Moon

14 DRO DEPARTURE
Leave DRO and start return to Earth

15 RETURN POWER FLY-BY (RPF)
RPF burn prep and return coast to Earth initiated

16 RETURN TRANSIT
Return Trajectory Correction (RTC) burns as necessary to aim for Earth's atmosphere; travel time 3-11 days

17 FINAL RETURN TRAJECTORY CORRECTION (RTC) BURN
Precision targeting for Earth entry

18 ENTRY INTERFACE (EI)
Enter Earth's atmosphere

19 SPLASHDOWN
Pacific Ocean landing within view of the U.S. Navy recovery ships

A B C D
CUBESATS DEPLOY
ICPS deploys 13 CubeSats total

Launch | Earth Orbit | Trans Lunar | Lunar Orbit | Trans Earth | Earth Re-entry | Payload Orbit/Disposal

Total distance traveled: 1.3 million miles – Mission duration: 26-42 days – Re-entry speed: 24,500 mph (Mach 32) – 13 CubeSats deployed

Artemis Mission and Getting Boots on the Moon

AMS Seminar 3/18/22

Orion Launch Abort System

- Artemis missions will return humans to the Moon and enable future manned missions to Mars. Delivering the necessary assets requires new powerful launch vehicles like the Space Launch System (SLS)

- NASA Advanced Supercomputing (NAS) Division at NASA Ames Research center is supporting multiple CFD efforts to enhance mission success

AMS Seminar 3/24/22

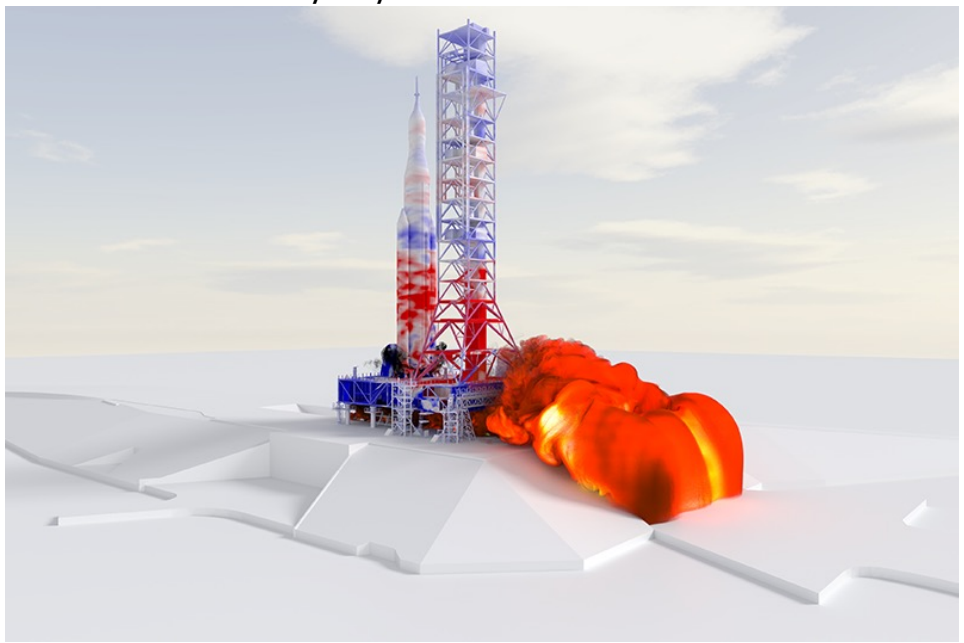

SLS Launch Environment

AMS Seminar 3/31/22

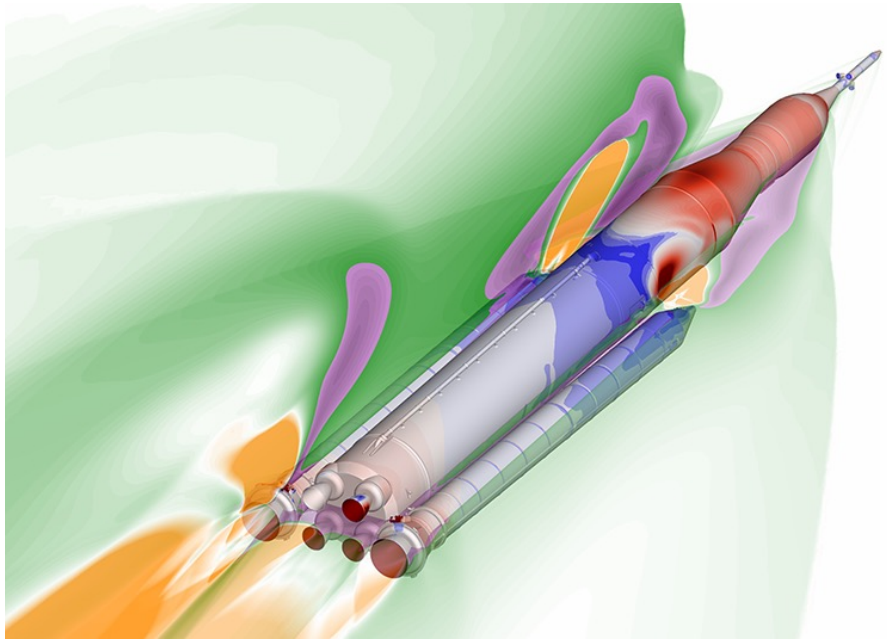

SLS Ascent Aerodatabase and Booster Separation

Artemis Mission and Getting Boots on the Moon

AMS Seminar 3/18/22

AMS Seminar 3/24/22

- Artemis missions will return humans to the Moon and enable future manned missions to Mars. Delivering the necessary assets
  ace Launch
  at NASA Ames
  s to enhance
  1/22

Orion Launch Abort System

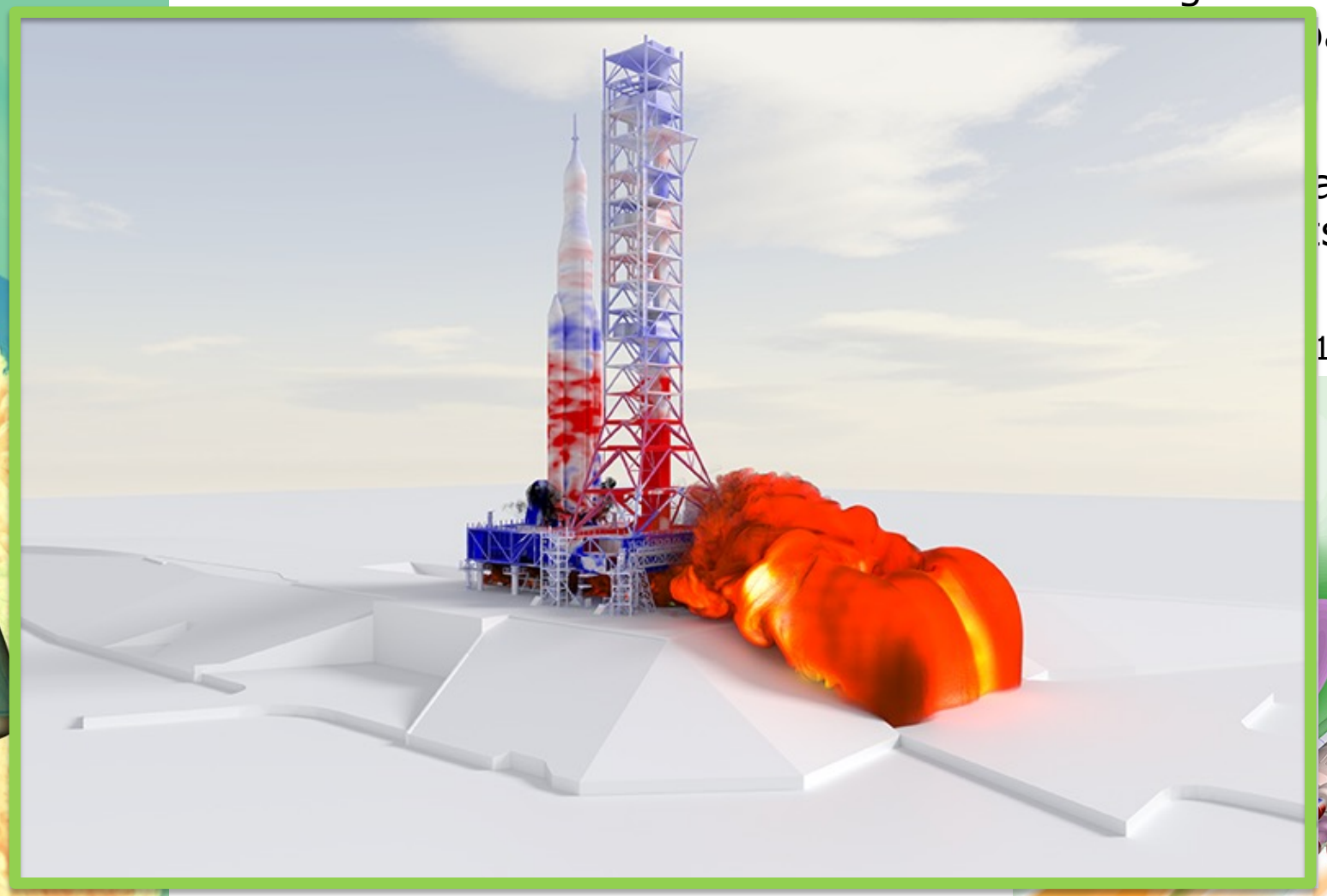

SLS Launch Environment

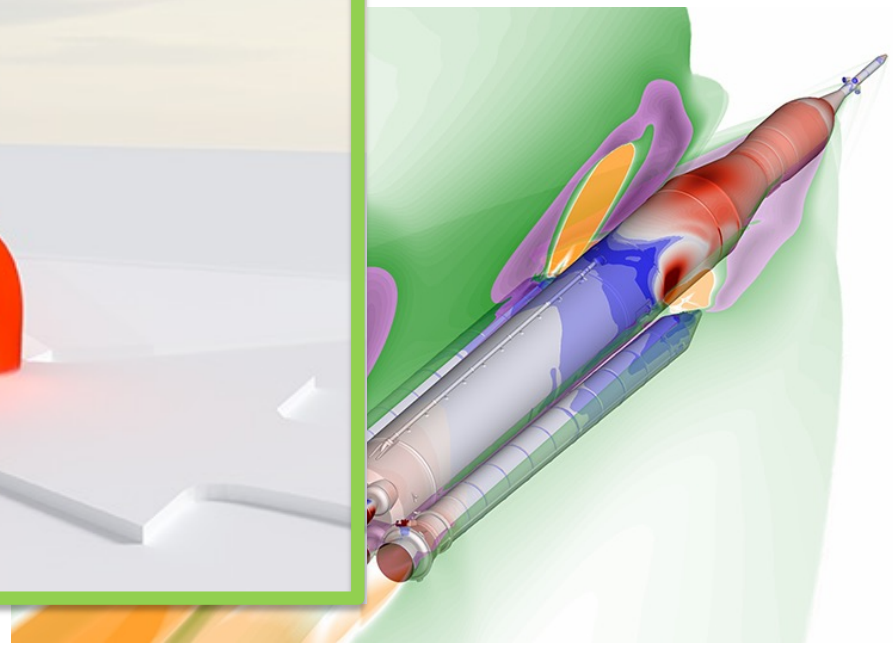

SLS Ascent Aerodatabase and Booster Separation

Computational Fluid Dynamics for Launch Environments

Ignition Overpressure Wave for STS-1 (1981)

- Launch vehicles experience strongest acoustic loads during ignition and lift off, vibrations can be dangerous if unmitigated
- Acoustic waves arise from different physical mechanisms
  - Broadband frequency noise from supersonic shear layers and supersonic impingement of plumes onto deflector and launch pad
  - Lower frequency, high-amplitude ignition overpressure caused by engine ignition and supersonic plume front acting like piston on ambient atmosphere

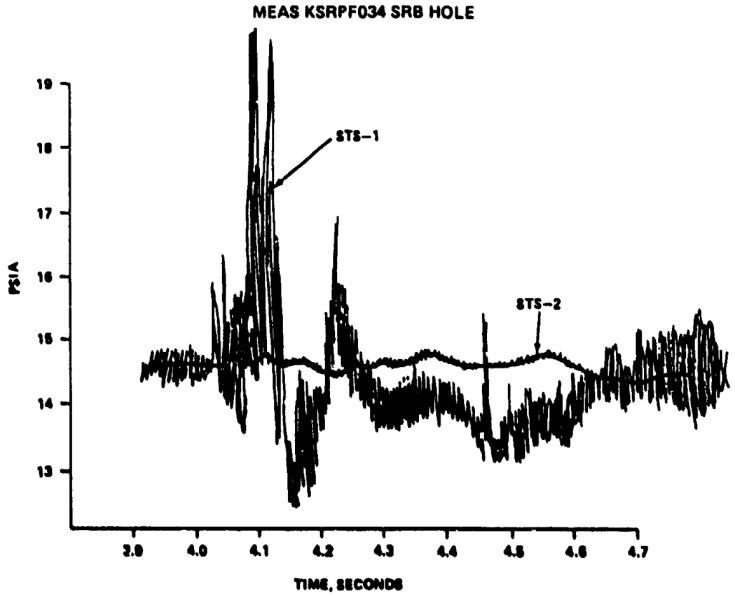

Figure 38. Shuttle overpressure data on LC39 launch facility.

NASA NTRS

	line cutter failed
STS-1/SRB/9	Ignition overpressure significantly larger than predicted
STS-1/SSME/1	Channel A and B MCC PC drift

"Shuttle flight data and in-flight anomaly list. STS-1 through STS-50, and STS-52 through STS-56. Revision T", 1993

Damage to LC-39A Flame Trench During STS-124 (2008)

STS-124 launch caused severe damage to flame trench sidewall, knocking loose dozens of bricks and scattering them down range of the pad

CFD Prediction of Ignition Overpressure Waves (2008 Simulations with Overset Grids)

- Shuttle era CFD flame trench and IOP/DOP studies performed using structured curvilinear overset grids
- Structured overset can grids provide excellent solution quality and are computationally efficient
- Reduced geometric fidelity to accommodate grid generation, which could take multiple months

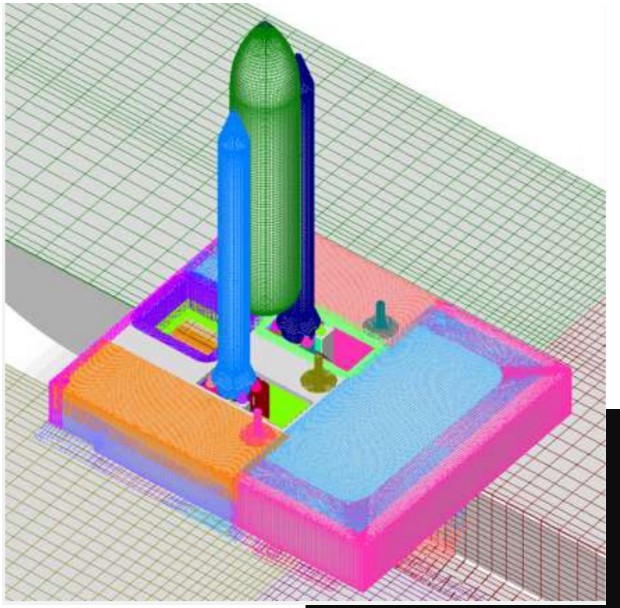

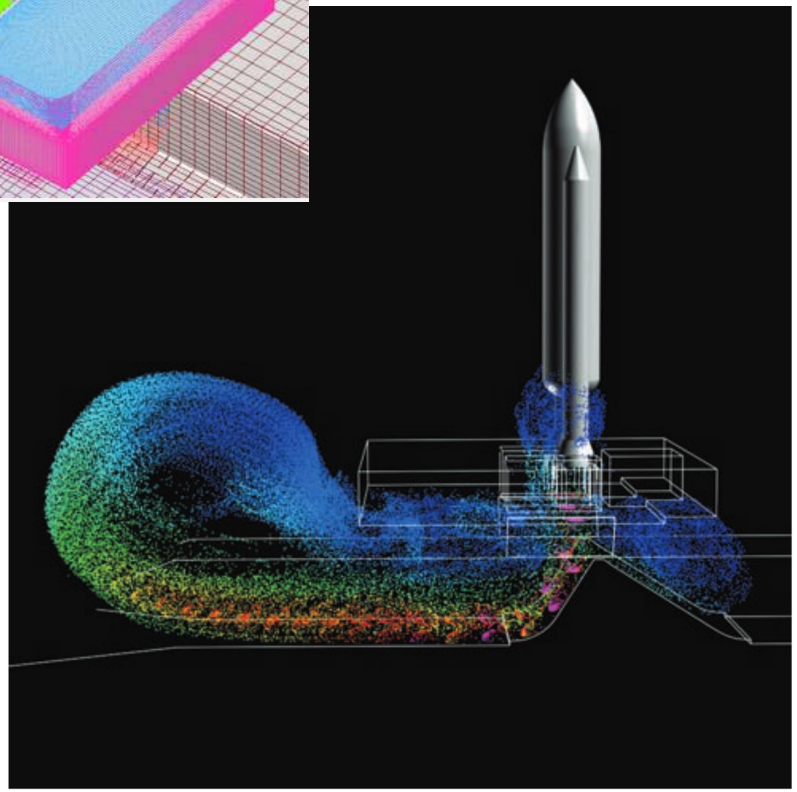

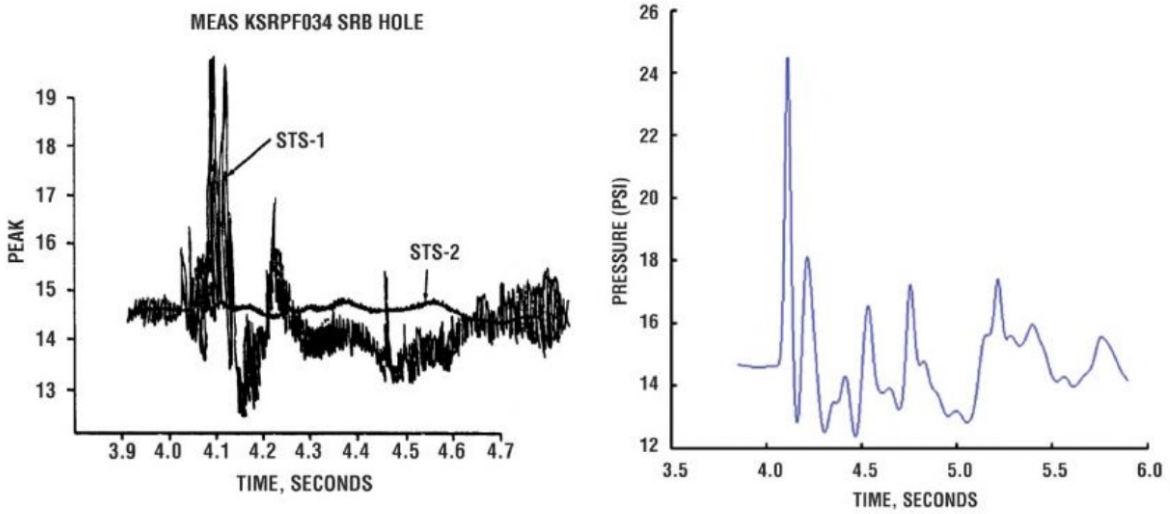

Kiris et al. "Time-Accurate Computational Analysis of the Flame Trench", 2009

Choosing Appropriate Grid Paradigm for Launch Environment

Structured Curvilinear

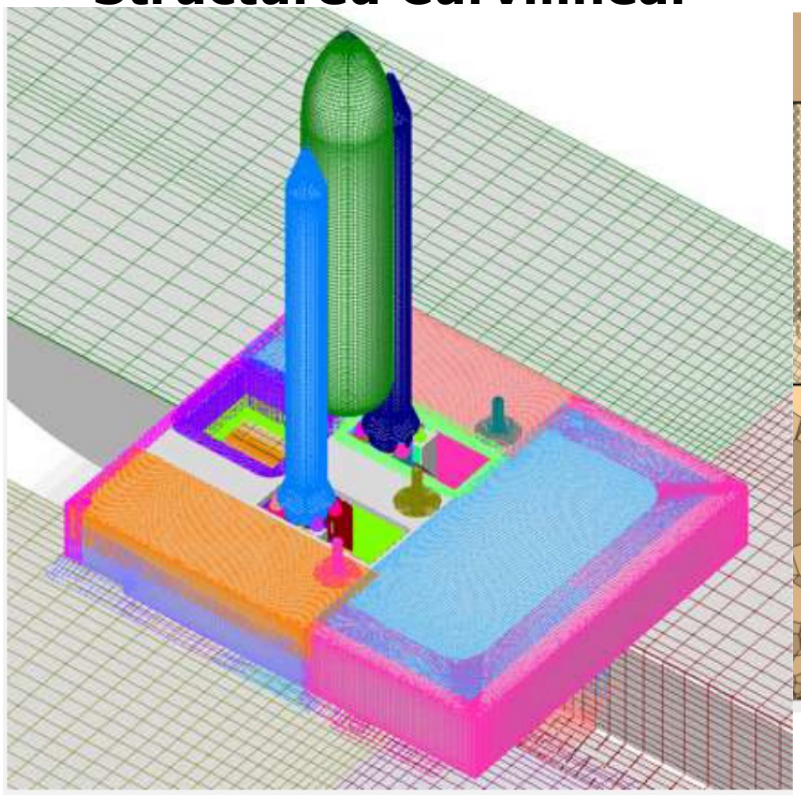

- Logically rectangular grids are efficient, high-order methods common
- Grid generation usually labor intensive, judging grid quality may require expertise

Unstructured

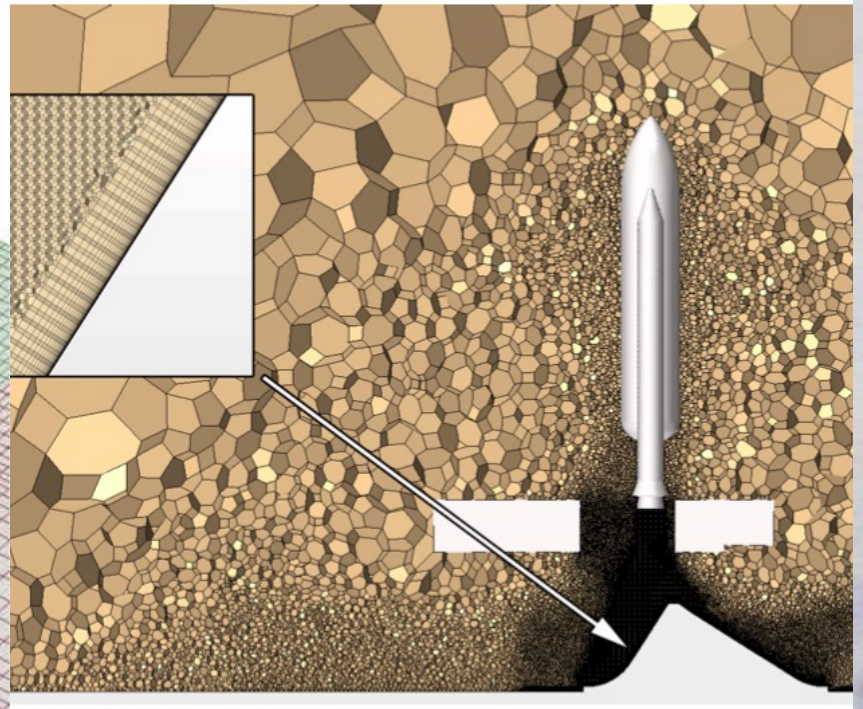

- Robust grid generation for complex geometry
- High-order methods non-trivial, computationally expensive

Cartesian

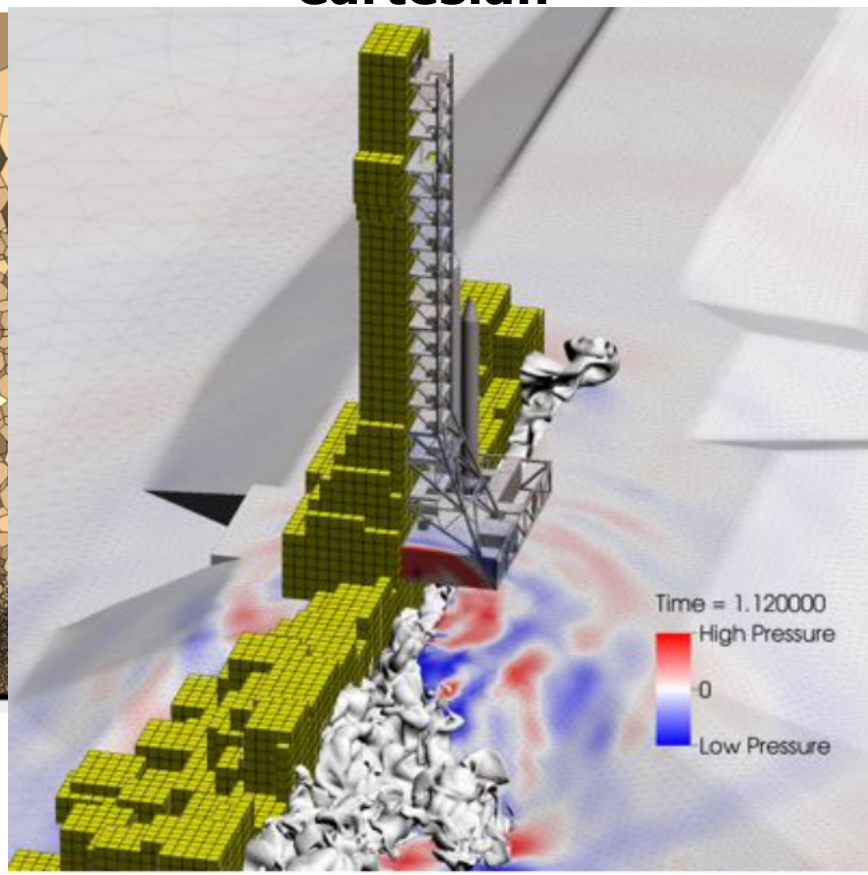

- Automatic volume grid generation
- High-order methods are efficient and mature
- Isotropic grid cells nonideal for boundary layer resolution

Launch, Ascent, Vehicle Aerodynamics (LAVA) Framework

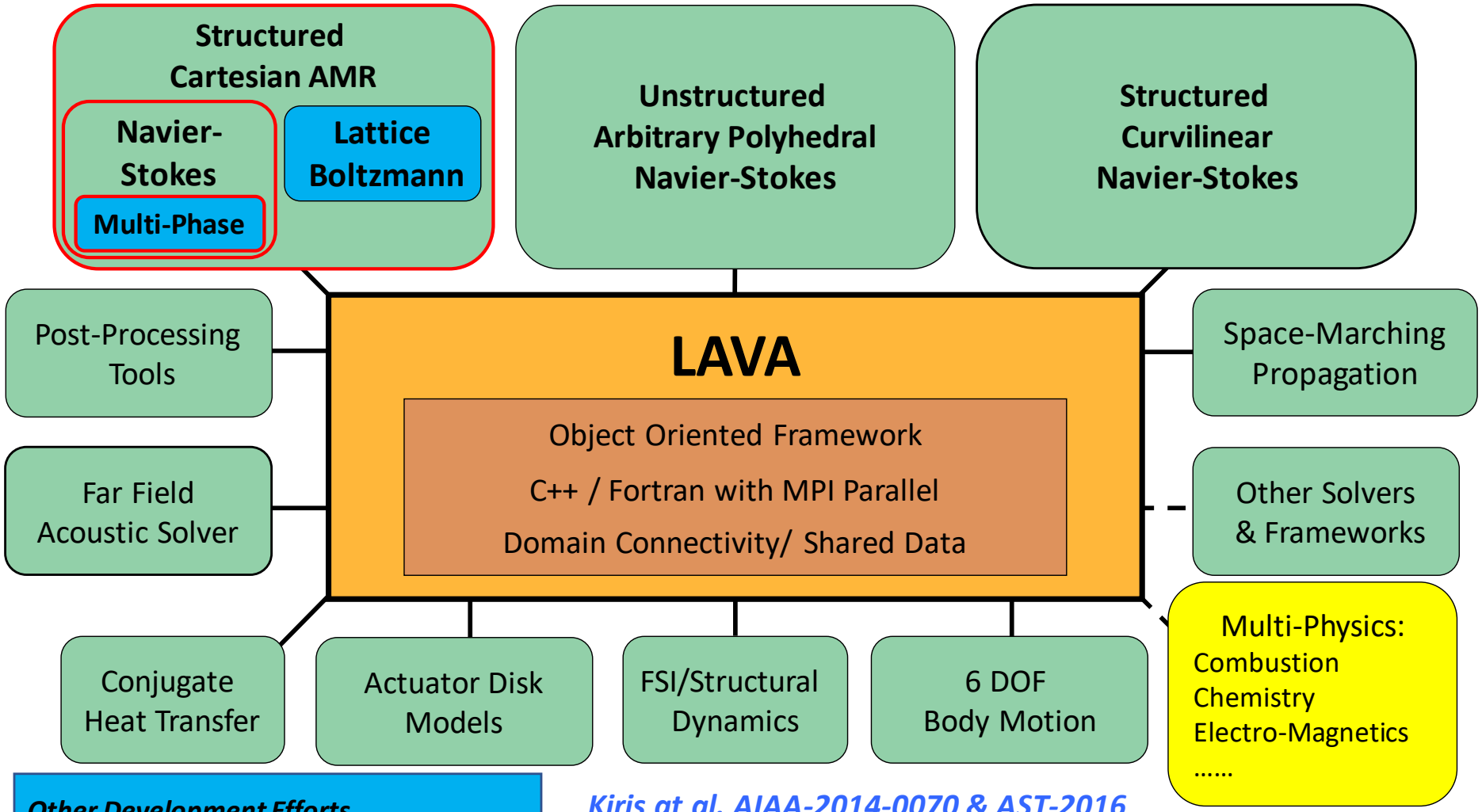

Other Development Efforts

- Higher order and low dissipation
- Curvilinear grid generation
- Wall modeling
- LES/DES/ILES Turbulence
- HEC (optimizations, accelerators, etc)

Kiris at al. AIAA-2014-0070 & AST-2016

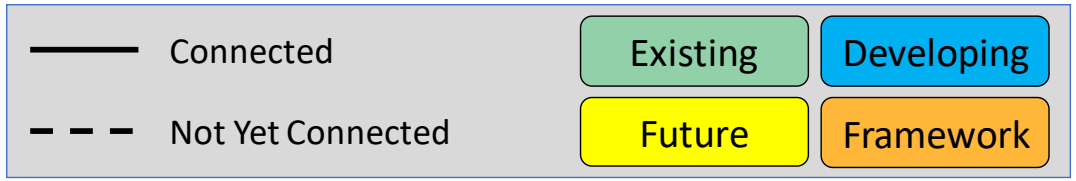

LAVA Structured Cartesian Launch Environment (2012 Simulations with Single Phase)

- Early validation efforts for LAVA Cartesian to simulate launch environment. Predicting pressure on main flame deflector
- Data from STS-135 launch; reasonable agreement to recorded pressure

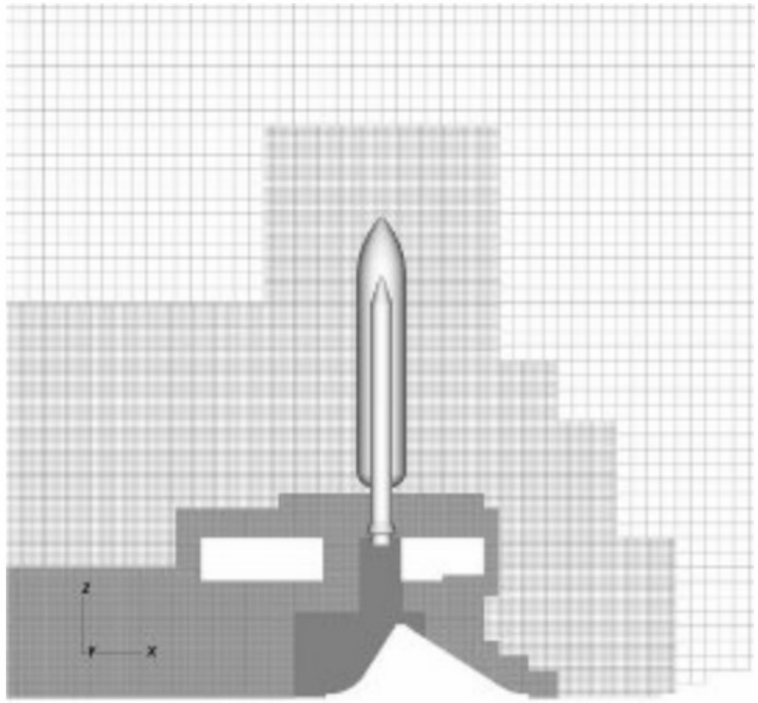

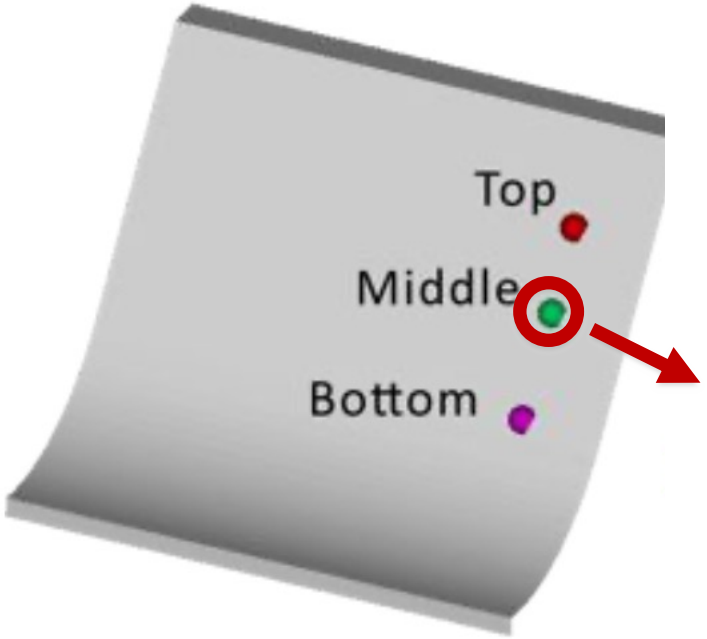

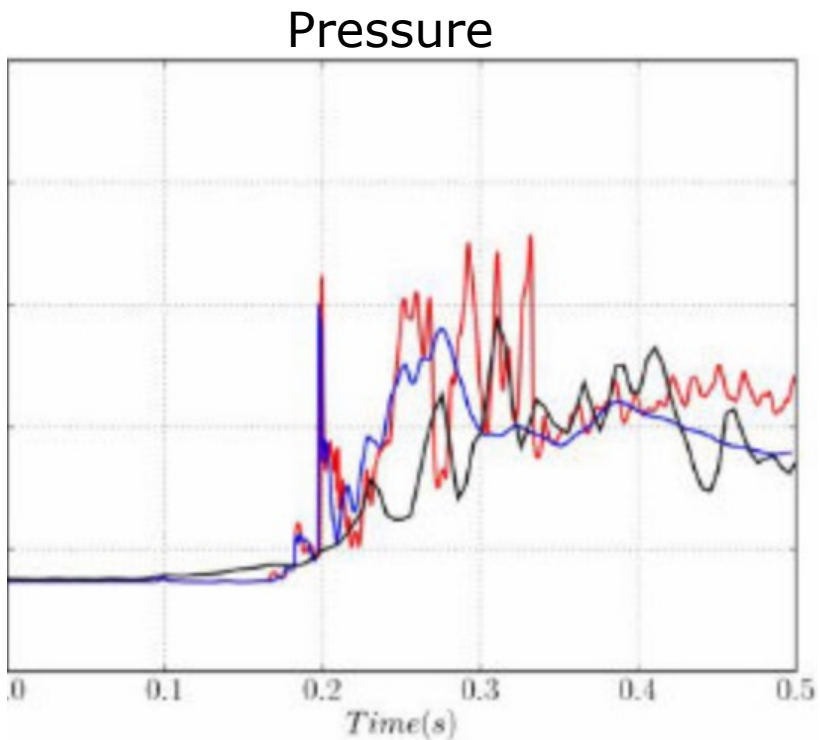

Unsteady pressure history at middle sensor location on MFD. Filtered flight data (black), LAVA-Unstructured viscous (blue) and LAVA-Cartesian inviscid (red) are shown.

S. Moini-Yekta et al. "Towards Hybrid Grid Simulations of the Launch Environment", ICCFD7, 2012

LAVA Structured Cartesian Launch Environment (2014 Simulations with Single Phase)

- LAVA Structured Cartesian solver ideal for inviscid flow design optimization where geometry may be changing between design iterations
- The LAVA solver was used extensively for the redesign efforts of the KSC launch pad for SLS

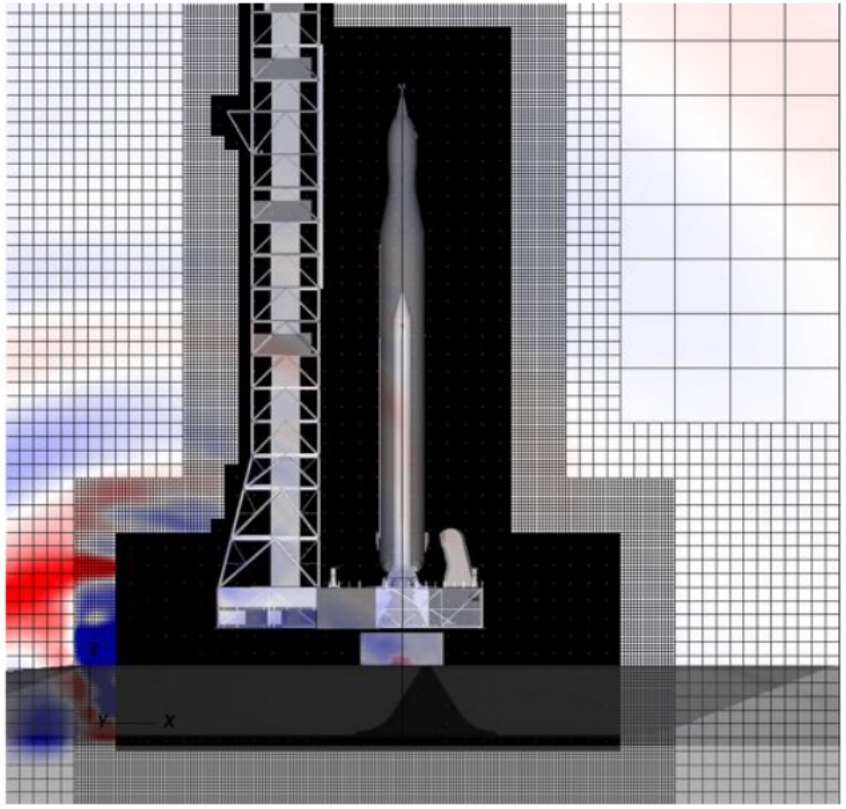

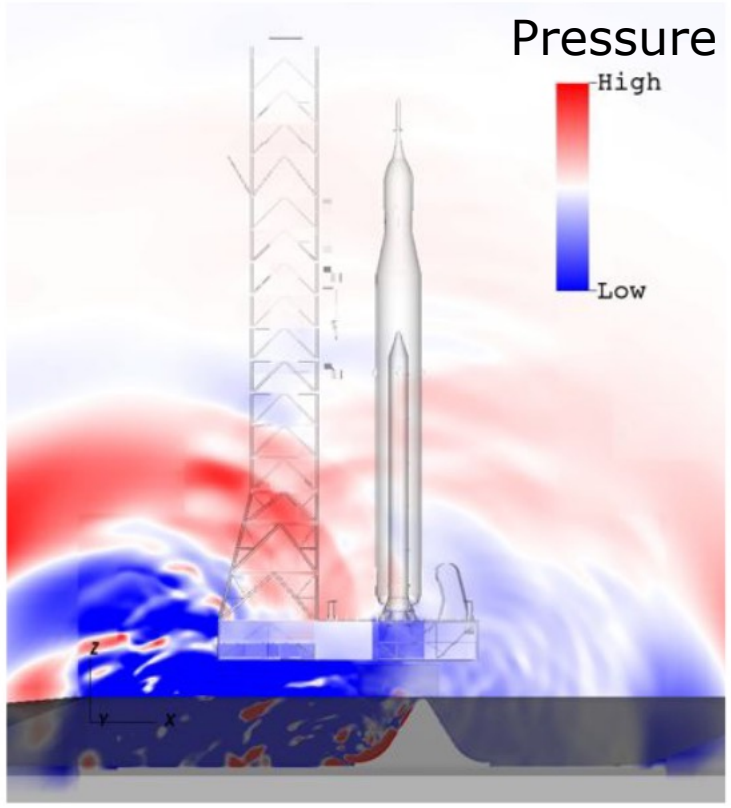

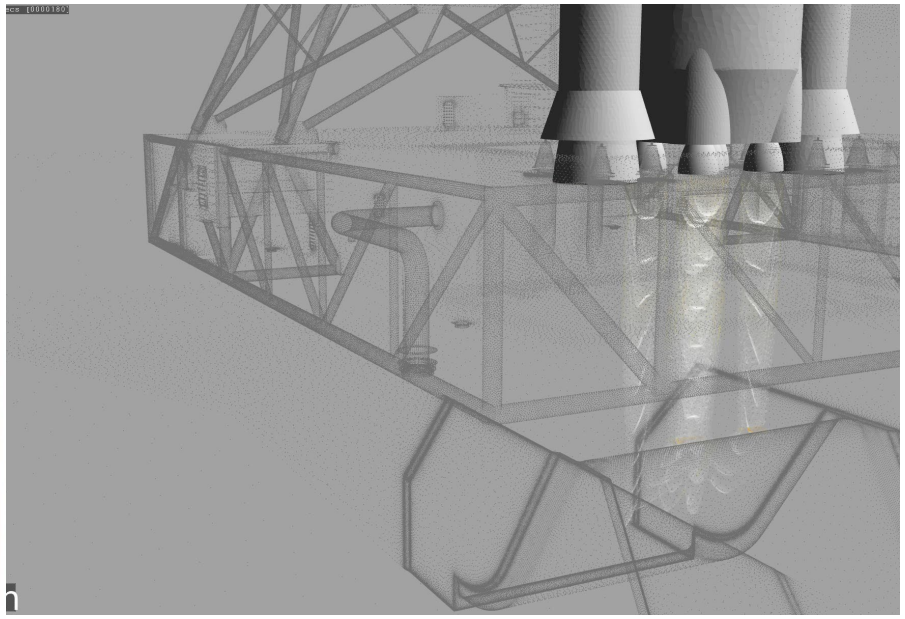

Kiris et al. "The LAVA Computational Fluid Dynamics Solver", AIAA SciTech Forum 2014

LAVA Structured Cartesian Launch Environment

Mach number

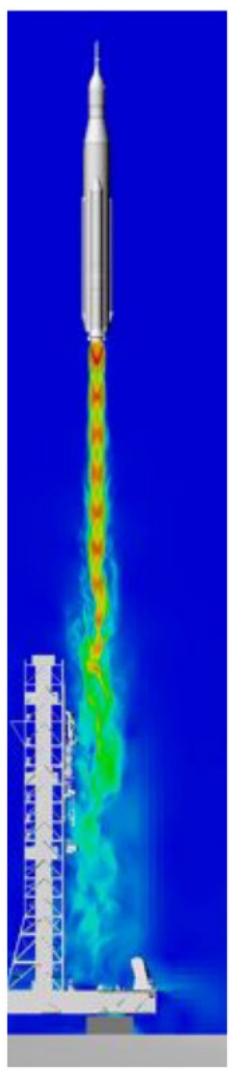

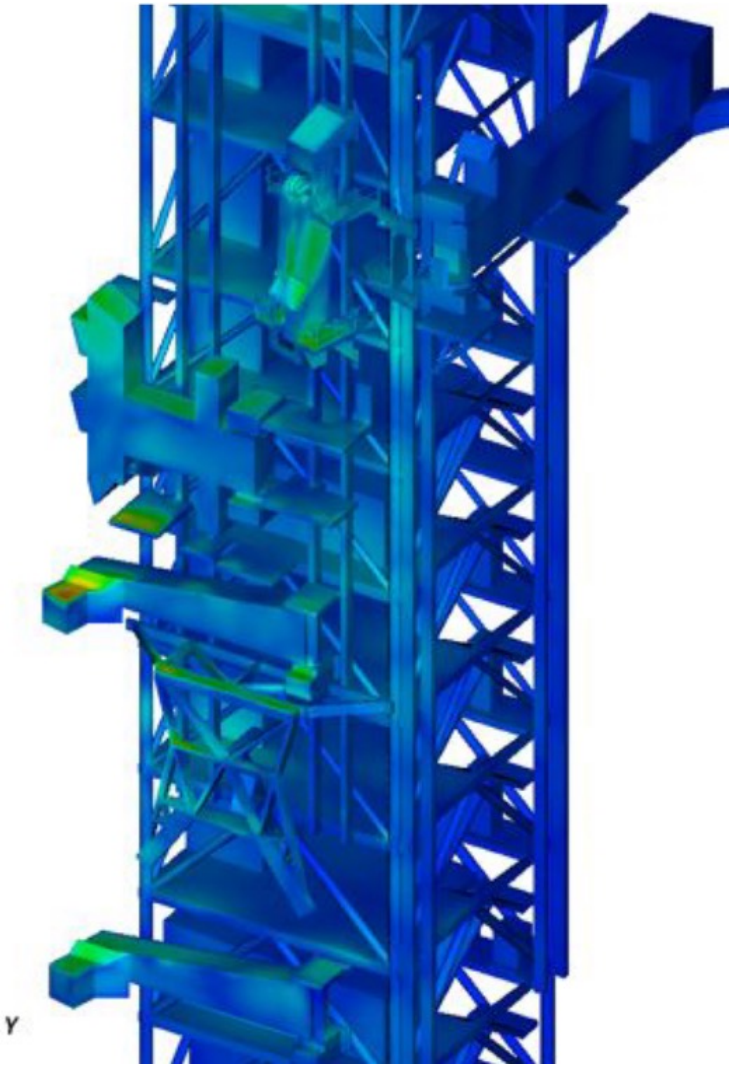

Maximum surface pressure

Examining Acoustic Loads on Launch Structures

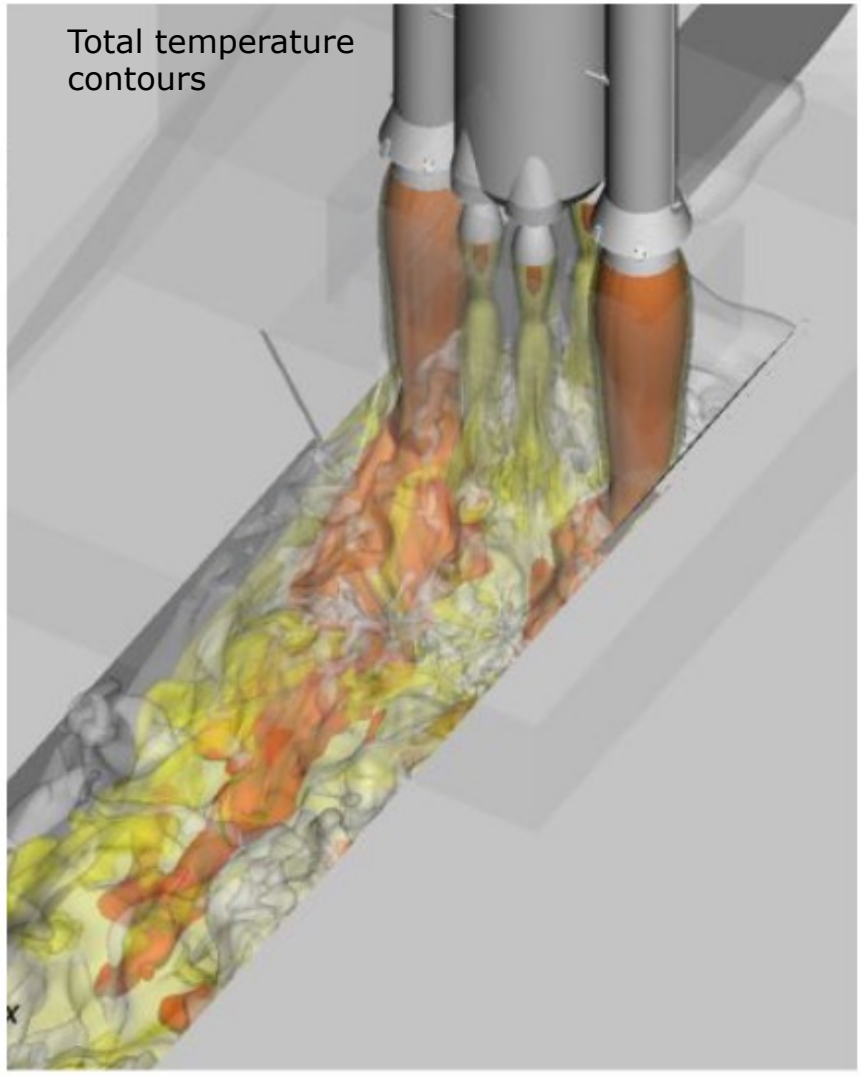

Plume Containment for Redesigned Flame Deflector

Kiris et al. "The LAVA Computational Fluid Dynamics Solver", AIAA SciTech Forum 2014

Main Flame Deflector Redesign at LC-39B

Courtesy of NASA KSC

- Supporting larger launch vehicles required an improved flame deflector
- New steel shingle deflector with finer geometric details and small gaps between deflector and wall
- Gaps may allow plume to spill behind deflector

M. Barad "High-Resolution Launch Environment Simulations". Supercomputing 2018

Efficient Immersed Boundary Cartesian Methods for Complex Geometry (2018)

No. Cells	No. Cores	Model	Runtime
550M	4000	Skylake	~5 weeks

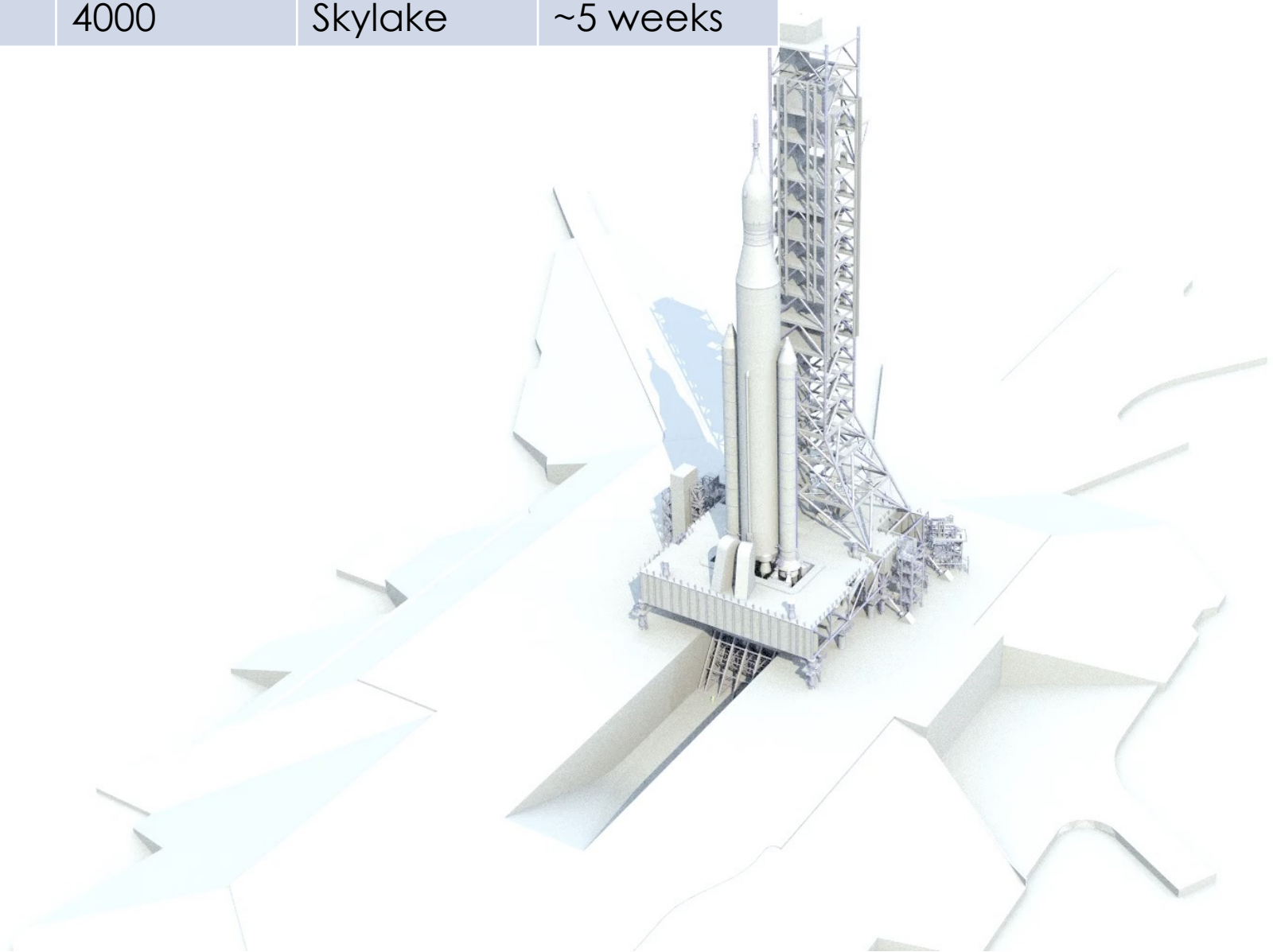

Towards Multiphase Simulations to Include Water-Based Sound Suppression Systems

Challenges in Modelling Water-Based Sound Suppression Systems

- **Plumes and the water system**: This is a highly nonlinear interaction involving very strong shock and expansion waves. The shocks pass through gas-water interfaces that have a density ratio of 1000:1.

- **Multiple scales**: Pressures generated inside the flame trench are orders of magnitude greater than the signal felt on the vehicle. It is necessary to predict the very extreme environment inside the trench and still capture the relatively weak signals that travel to the vehicle.

Goal: Multiphase CFD capability for accurate and reliable predictions of IOP with water-based sound suppression systems

Governing Equations for Multiphase Flow

Equations of motion for 2 fluids with single velocity and single pressure proposed by Allaire (five-equation model)

$$\partial_t (\alpha_1 \rho_1) + \nabla \cdot (\alpha_1 \rho_1 \mathbf{u}) = 0 \quad \text{Conservation of Species 1 Mass}$$

$$\partial_t (\alpha_2 \rho_2) + \nabla \cdot (\alpha_2 \rho_2 \mathbf{u}) = 0 \quad \text{Conservation of Species 2 Mass}$$

$$\partial_t (\rho \mathbf{u}) + \nabla \cdot (\rho \mathbf{u} \otimes \mathbf{u}) + \nabla p = 0 \quad \text{Conservation of Mixture Momentum}$$

$$\partial_t E + \nabla \cdot [(E + p)\,\mathbf{u}] = 0 \quad \text{Conservation of Mixture Energy}$$

$$\partial_t \alpha_1 + \mathbf{u} \cdot \nabla \alpha_1 = 0 \quad \text{Nonconservative Transport Equation}$$

with additional constraints:

$$\alpha_1 + \alpha_2 = 1 \qquad \alpha_1 \rho_1 + \alpha_2 \rho_2 = \rho \qquad \alpha_1 \rho_1 e_1 + \alpha_2 \rho_2 e_2 = \rho e$$

Stiffened gas equation of state for each phase proposed by Harlow

$$p_k + \gamma_k p_k^{\infty} = \rho_k e_k (\gamma_k - 1)$$

Mechanical equilibrium assumption gives equation for single mixture pressure

Wong et al. "A positivity-preserving high-order weighted compact nonlinear scheme for compressible gas-liquid flows" Journal of Computational Physics, 2021

Physically Admissible Solution Space

- For the launch environment, conditions may be very extreme with strongly nonlinear shocks and rarefactions waves interacting with material interfaces with huge density gradients
- Common mode of failure for numerical methods with these kinds of interactions is failure to predict a real speed of sound ($c^2 < 0$). This leads to loss of hyperbolicity and ill-posed equations
- We adopt a strategy based on previous work for Euler's equations to devise numerical procedures that are provably positivity-preserving
- Define set of *admissible states* such that all solution vectors in that set have positive densities and a real speed of sound

$$G = \left\{ \mathbf{W} = \begin{pmatrix} \alpha_1\rho_1 \\ \alpha_2\rho_2 \\ \rho\mathbf{u} \\ E \\ \alpha_1 \end{pmatrix}, 0 < \alpha_k < 1,\ \alpha_k\rho_k > 0,\ \rho c^2 > 0 \right\}$$

Wong et al. "A positivity-preserving high-order weighted compact nonlinear scheme for compressible gas-liquid flows" Journal of Computational Physics, 2021
Hu et al. "Positivity-preserving method for high-order conservative schemes solving compressible Euler equations." *Journal of Computational Physics*, 2013.

Novel Robust Method for Multiphase Simulations

Define Admissible Set of Solutions

First-order HLLC Scheme Positivity Preserving

Derive High-Order WCNS Procedure

Flux Limiting for High-Order Positivity Preserving Scheme

$$G = \left\{ \mathbf{W} = \begin{pmatrix} \alpha_1\rho_1 \\ \alpha_2\rho_2 \\ \rho\mathbf{u} \\ E \\ \alpha_1 \end{pmatrix}, 0 < \alpha_k < 1,\ \alpha_k\rho_k > 0,\ \rho c^2 > 0 \right\}$$

Lemma 1: G is a convex set i.e.; *G is closed under convex combinations of elements in G*

Wong et al. "A positivity-preserving high-order weighted compact nonlinear scheme for compressible gas-liquid flows" Journal of Computational Physics, 2021

Novel Robust Method for Multiphase Simulations

Define Admissible Set of Solutions

First-order HLLC Scheme Positivity Preserving

Derive High-Order WCNS Procedure

Flux Limiting for High-Order Positivity Preserving Scheme

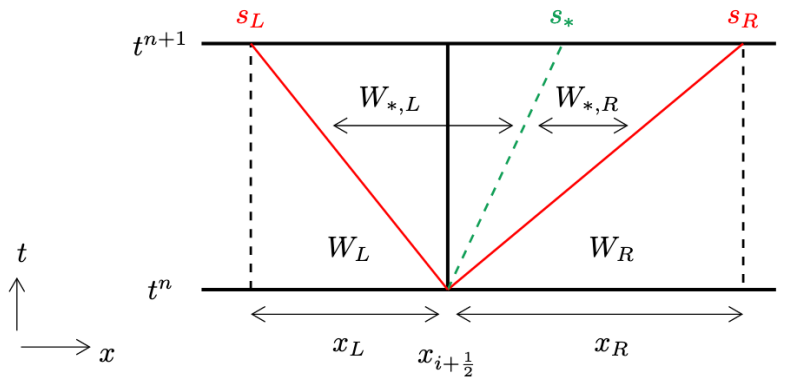

$$\mathbf{W}_i^{n+1} = \mathbf{W}_i^n - \frac{\Delta t}{\Delta x}\left(\hat{\mathbf{G}}^-_{i+\frac{1}{2}} - \hat{\mathbf{G}}^+_{i-\frac{1}{2}}\right)$$

$$\hat{\mathbf{G}}^{\pm}_{i\mp\frac{1}{2}} = \hat{\mathbf{G}}_{i\mp\frac{1}{2}} - \alpha_{1i}\begin{pmatrix}0 & 0 & 0 & 0 & \hat{u}_{i\mp\frac{1}{2}}\end{pmatrix}^T$$

Lemma 2: The HLLC approximate Riemann solver produces a star state in G if left and right states are also in G

Theorem: Under suitable CFL condition, the first-order scheme using the HLLC approximate Riemann solver produces an updated state that is in G.

Wong et al. "A positivity-preserving high-order weighted compact nonlinear scheme for compressible gas-liquid flows" Journal of Computational Physics, 2021

Novel Robust Method for Multiphase Simulations

Define Admissible Set of Solutions

First-order HLLC Scheme Positivity Preserving

Derive High-Order WCNS Procedure

Flux Limiting for High-Order Positivity Preserving Scheme

- Write system in method-of-lines semi-discretization

$$\frac{\mathrm{d}}{\mathrm{d}t}u_i = -\left(\frac{\partial \mathbf{F}}{\partial x}\right)_i$$

- Hybrid explicit centered compact scheme for high-order evaluation of flux divergence

- Reconstruct high-order fluxes at cell faces for provable discrete conservation (except volume fraction equation)

$$\left(\frac{\partial \mathbf{G}}{\partial x}\right)_i = \frac{\tilde{\mathbf{G}}^{-}_{i+\frac{1}{2}} - \tilde{\mathbf{G}}^{+}_{i-\frac{1}{2}}}{\Delta x}$$

- High-order accurate velocity and numerical flux reconstruction at cell faces constructed with robust WENO interpolation and HLLC Riemann solver

Wong et al. "A positivity-preserving high-order weighted compact nonlinear scheme for compressible gas-liquid flows" Journal of Computational Physics, 2021

Novel Robust Method for Multiphase Simulations

Define Admissible Set of Solutions

First-order HLLC Scheme Positivity Preserving

Derive High-Order WCNS Procedure

Flux Limiting for High-Order Positivity Preserving Scheme

- Limit high-order reconstructed variables at cell faces

$$\left(1-\theta_{i+\frac{1}{2}}\right)\rho c^2\left(\mathbf{W}_i\right)+\theta_{i+\frac{1}{2}}\rho c^2\left(\tilde{\mathbf{W}}_{i+\frac{1}{2}}\right)=\epsilon$$

$$\mathbf{W}^*_{i+\frac{1}{2}}=\left(1-\theta_{i+\frac{1}{2}}\right)\mathbf{W}_i+\theta_{i+\frac{1}{2}}\tilde{\mathbf{W}}_{i+\frac{1}{2}}$$

- Do this for partial densities, volume fractions, and sound speed squared
- Follow a similar limiting procedure for limiting the numerical flux so that the update is boundedness and positivity preserving

Wong et al. "A positivity-preserving high-order weighted compact nonlinear scheme for compressible gas-liquid flows" Journal of Computational Physics, 2021

Novel Robust Method for Multiphase Simulations

- Formally high-order accurate in smooth regions
- Stability shown for forward Euler timestep. Achieve high-order time accuracy by using Strong Stability Preserving (SSP) Runge-Kutta methods.
- These methods are linear multistep methods constructed from *convex combinations* of forward Euler steps
- This means each substep is positivity-preserving which makes the overall time integration also positivity-preserving
- We apply three stage, third-order SSP-RK for all multiphase calculations presented for the high-order WCNS scheme

ρ_1 (kg m^{-3})	ρ_2 (kg m^{-3})	u (m s^{-1})	v (m s^{-1})	p (Pa)	α_1
1000	1	10	10	101325	$0.5 + 0.25 \sin[\pi(x+y)]$

Number of	HLLC		PP-WCNS-IS	
grid points	error	order	error	order
8^2	4.283e−04		3.136e−05	
16^2	2.170e−04	0.98	1.517e−07	7.69
32^2	1.089e−04	0.99	4.855e−09	4.97
64^2	5.450e−05	1.00	1.679e−10	4.85
128^2	2.726e−05	1.00	5.382e−12	4.96
256^2	1.363e−05	1.00	1.714e−13	4.97

Convergence of volume fraction equation for smooth solution

Wong et al. "A positivity-preserving high-order weighted compact nonlinear scheme for compressible gas-liquid flows" Journal of Computational Physics, 2021

Shock Tube Calculations and Robustness Test

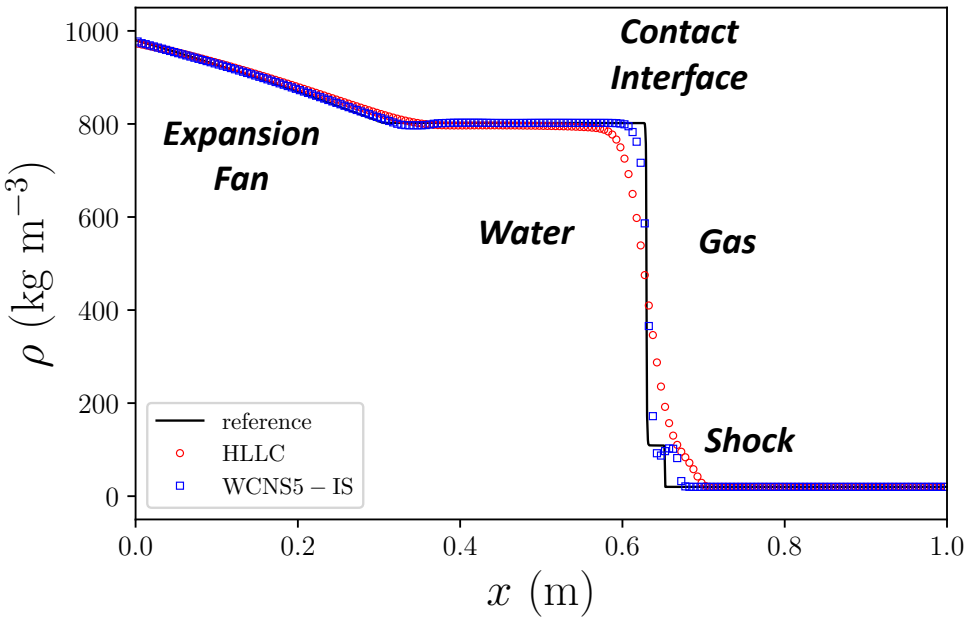

1D shock tube problem with air-water interface. Comparison of first-order HLLC scheme and high-order method

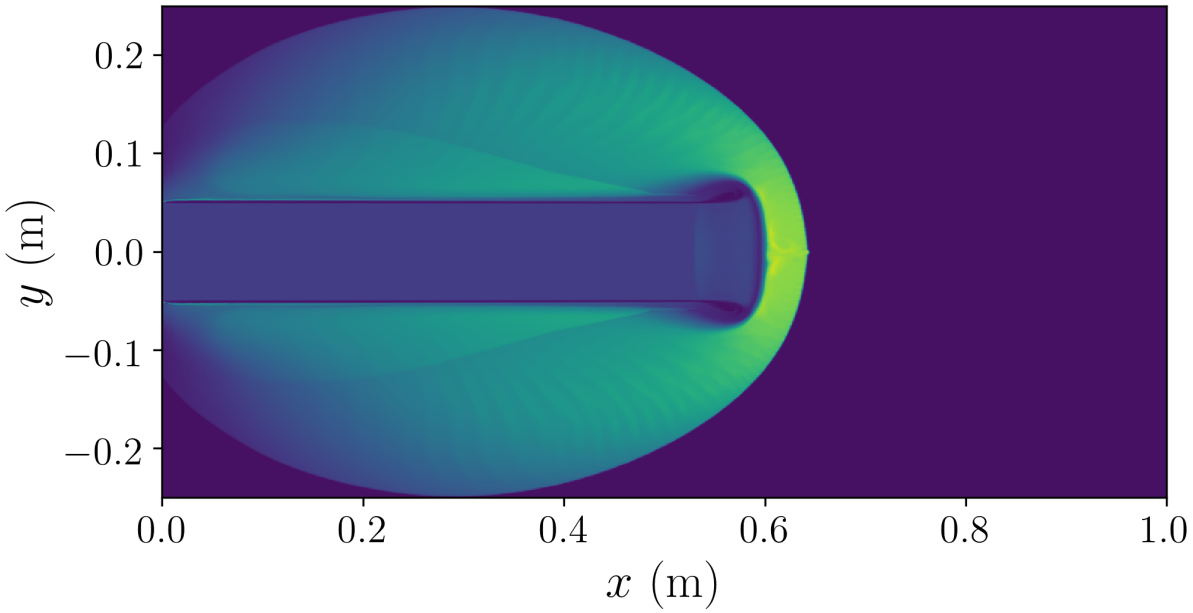

2D Mach 100 liquid water jet. Test of robustness

- Initial numerical experiments to assess the accuracy and robustness of the method
  - Shock tube problem with shock passing from liquid to air. Reflected expansion wave, weak transmitted shock near contact
  - Mach 100 liquid jet. Extreme problem to demonstrate robustness of the scheme and ability to accurately capture the liquid-air contact

Wong et al. "A positivity-preserving high-order weighted compact nonlinear scheme for compressible gas-liquid flows" Journal of Computational Physics, 2021

Shock/Water Column Interaction and Contact Resolution

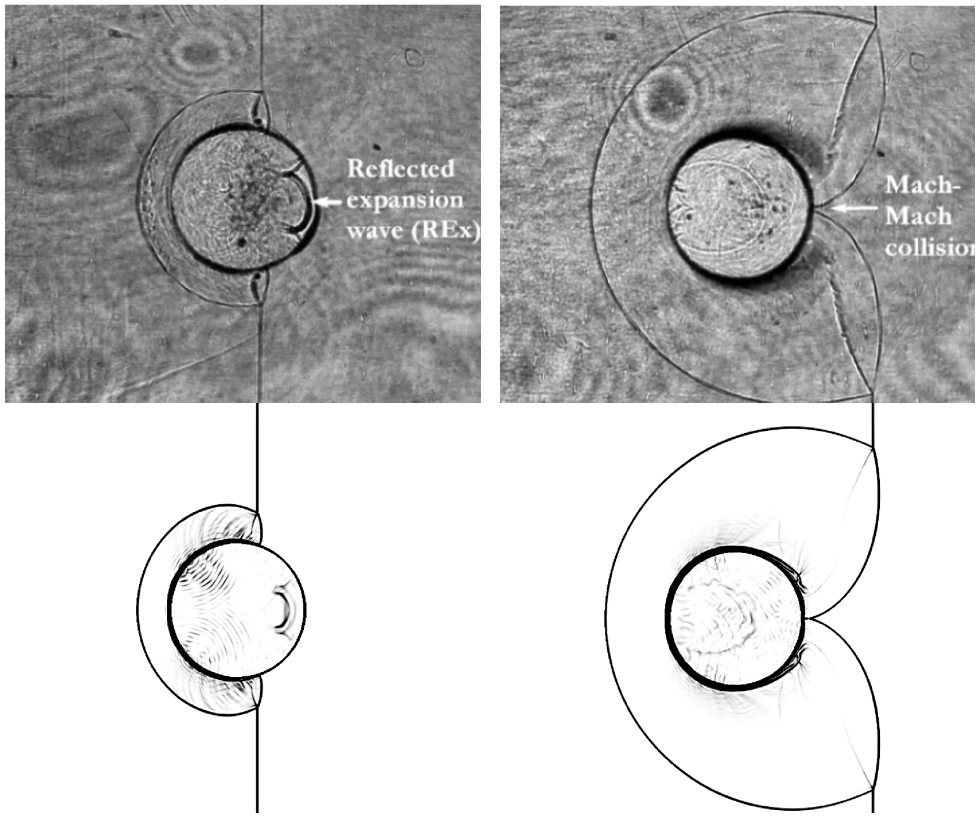

Validation case of a Mach 2.4 shock passing over a stationary water column. The top row shows shadowgraph images taken during the experiment and the bottom shows a Schlieren type plot for the numerical simulation.

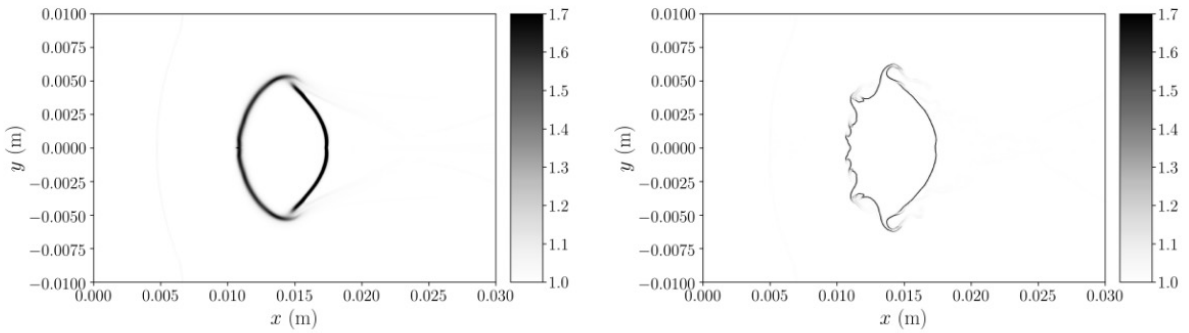

(g) $t = 16\ \mu$s, HLLC (h) $t = 16\ \mu$s, PP-WCNS-IS

Droplet interface post-shock

- Verification of wave dynamics for shocks and air-water interfaces
- High-order shows significant advantages in prediction of interface break-up at later times

S. Sembian et al. "Plane shock wave interaction with a cylindrical water column". *Physics of Fluids*, 2016.

Wong et al. "A positivity-preserving high-order weighted compact nonlinear scheme for compressible gas-liquid flows" Journal of Computational Physics, 2021

Phase Transition for Liquid/Vapor Mixtures

- To account for the vaporization of liquid water, we include water vapor as an additional species in our system of equations and modify equation of state to include a reference energy
- We say the liquid water and water vapor are in equilibrium if their Gibbs free energies are equal. In general, after a hyperbolic step the liquid water and water vapor are not in equilibrium
- Adapted phase transition procedure from Chiapolino originally formulated for four-equation multispecies model, easily extended to the five-equation system we solve
- Solve nonlinear equation (or estimate solution) for saturation conditions that gives an equilibrium pressure, temperature, and vapor mass fractions
- Positivity-preserving formulation for N species relies on thermal relaxation step. Manuscript in preparation

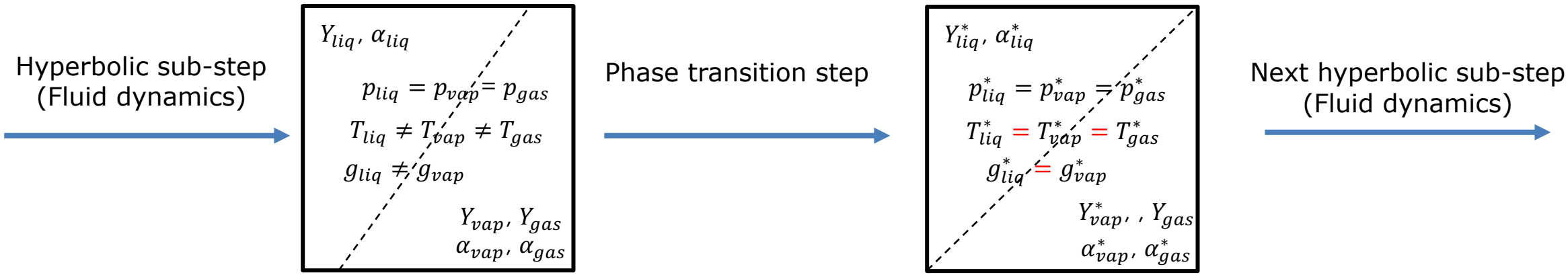

A. Chiapolino "A simple and fast phase transition relaxation solver for compressible multicomponent two-phase flows". *Computers & Fluids*, 2017

Validation of Multiphase Solver for Launch Vehicles

Simulating Falcon Heavy STP-2 Ignition (2021)

- STP-2 flight June 2019
- Pressure data available from flame trench ceiling and one pressure sensor on vehicle body
- 4% relative error in peak over pressure at body sensor

No. Cells	No. Cores	Model	Runtime
425M	8000	Skylake	~7.5 weeks

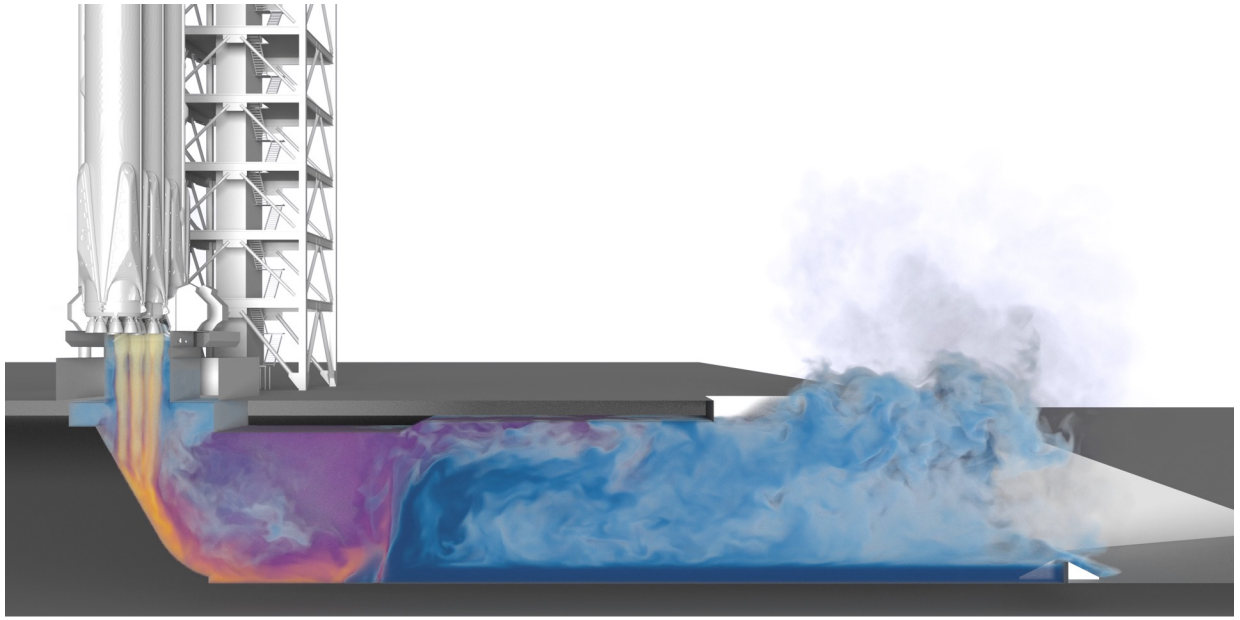

Simulating Falcon Heavy STP-2 Ignition (2021)

- STP-2 flight June 2019
- Pressure data available from flame trench ceiling and one pressure sensor on vehicle body
- 4% relative error in peak over pressure at body sensor

No. Cells	No. Cores	Model	Runtime
425M	8000	Skylake	~7.5 weeks

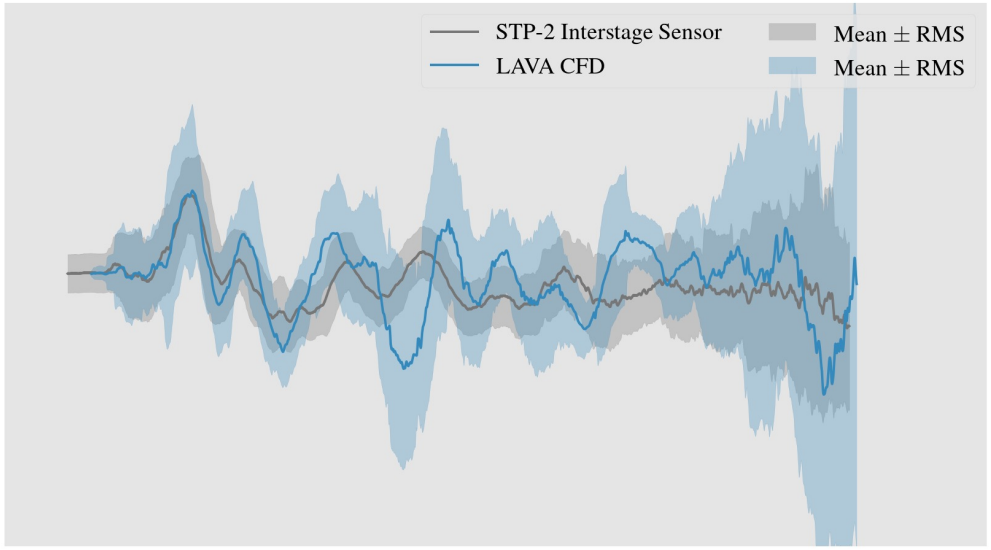

SLS Scale Model Acoustic Test (SMAT)

- Scale test at Marshall Space Flight Center provides extensive measurements of the launch environment to understand effectiveness of IOP/SS system
- SMAT case is ideal to validate the multiphase solver for future SLS missions
- Performed dry simulations first to validate geometry, boundary conditions, and problem setup
- Performed multiphase simulations including water with phase transition

Dry Run

Wet Run

www.nasa.gov/exploration/systems/sls/multimedia/images

SLS Scale Model Acoustic Test (SMAT)

Scale Model Acoustic Test (SMAT): Dry Simulations with LAVA (2021)

- Approx. 1M time steps for complete simulation
- Mesh has approx. 300M grid cells, finest resolution is 1mm near nozzle exits
- 2 time-dependent boundary conditions for solid booster exits, 4 steady boundary conditions for liquid thruster exits
- Numerical sensors placed throughout domain for comparison with available test measurements

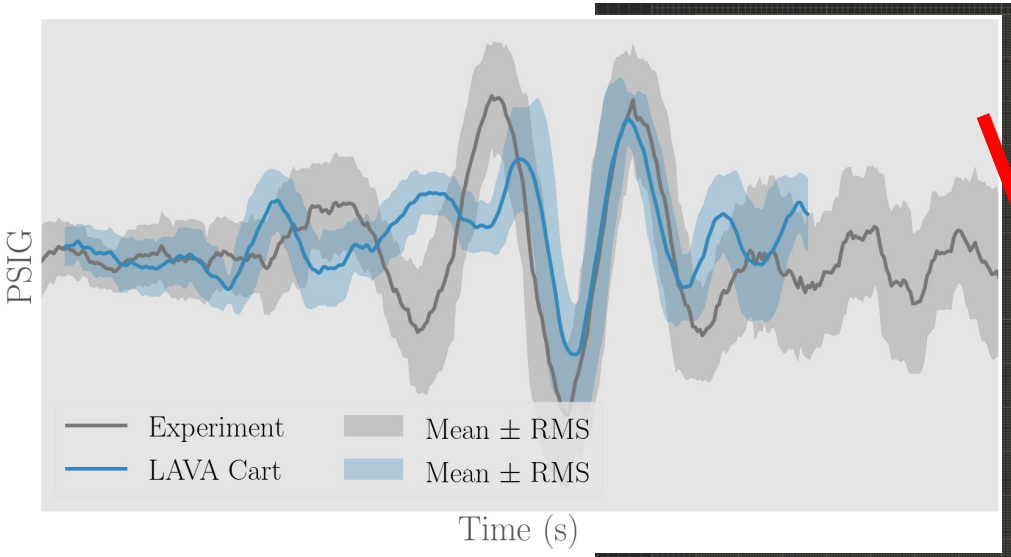

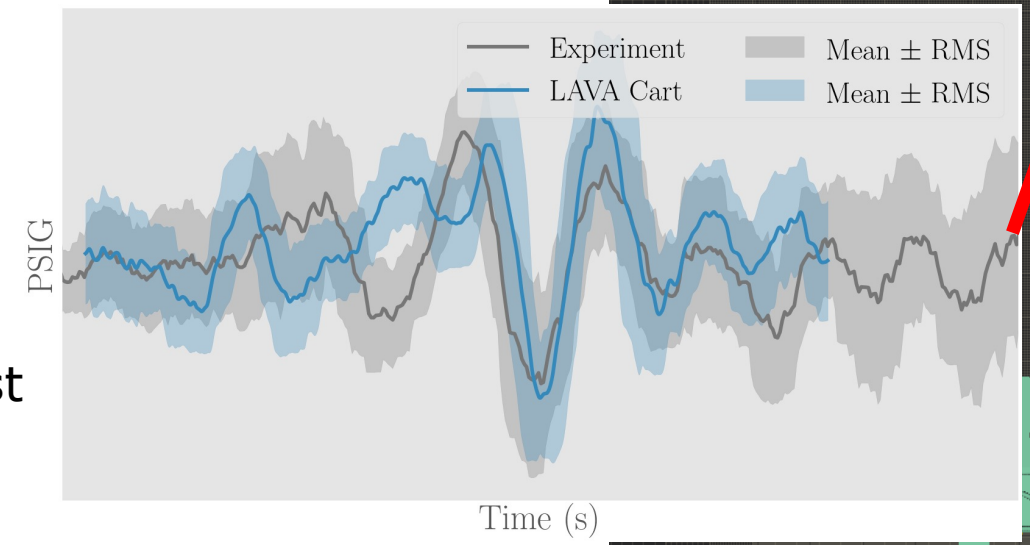

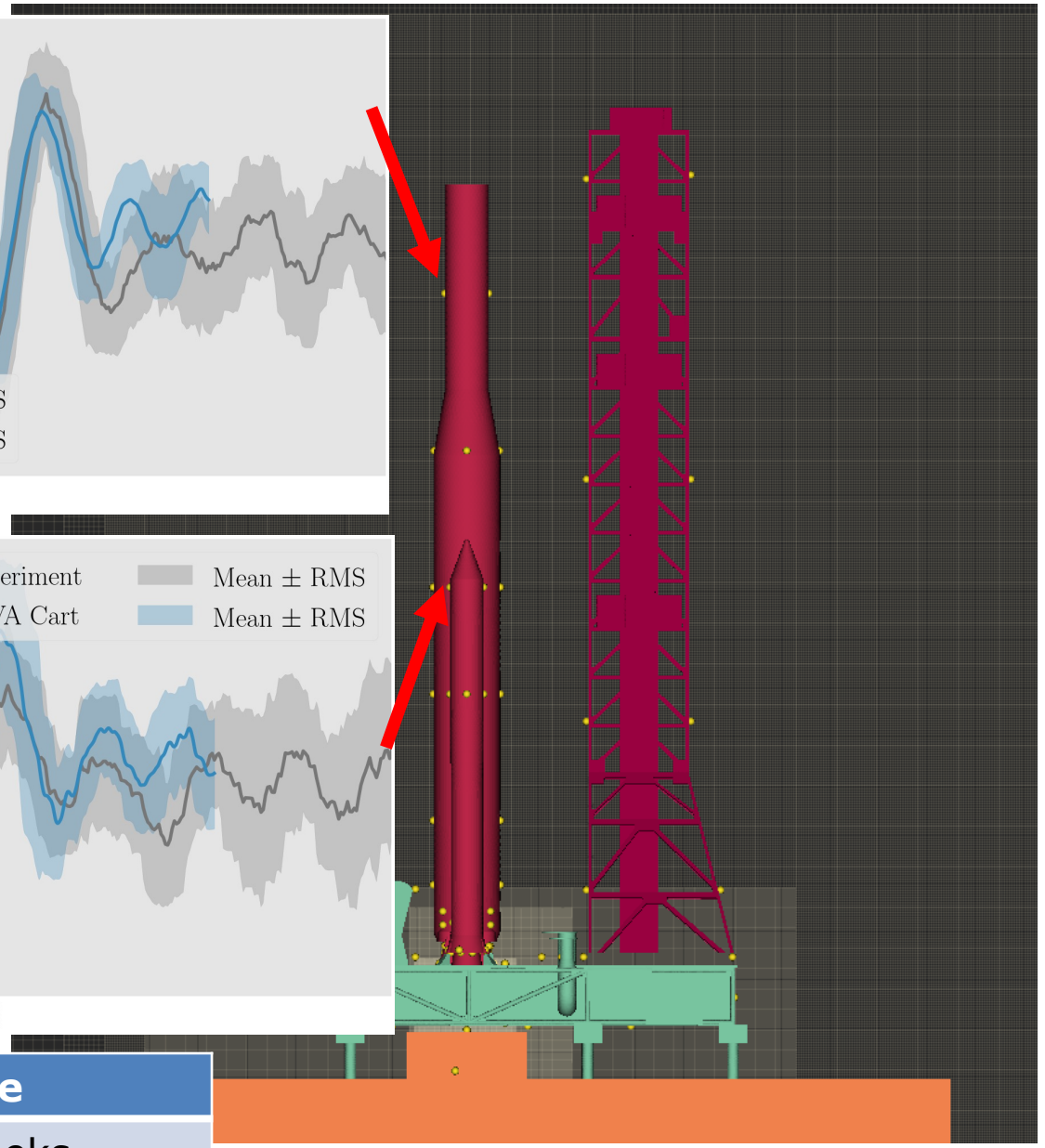

No. Cells	No. Cores	Model	Runtime
300M	8000	Skylake	~2.5 weeks

Scale Model Acoustic Test (SMAT): Wet Simulations with LAVA (2021)

- Multiphase CFD predicts a stronger underpressure
- Approx. 3M time steps due to multiphase CFL constraint

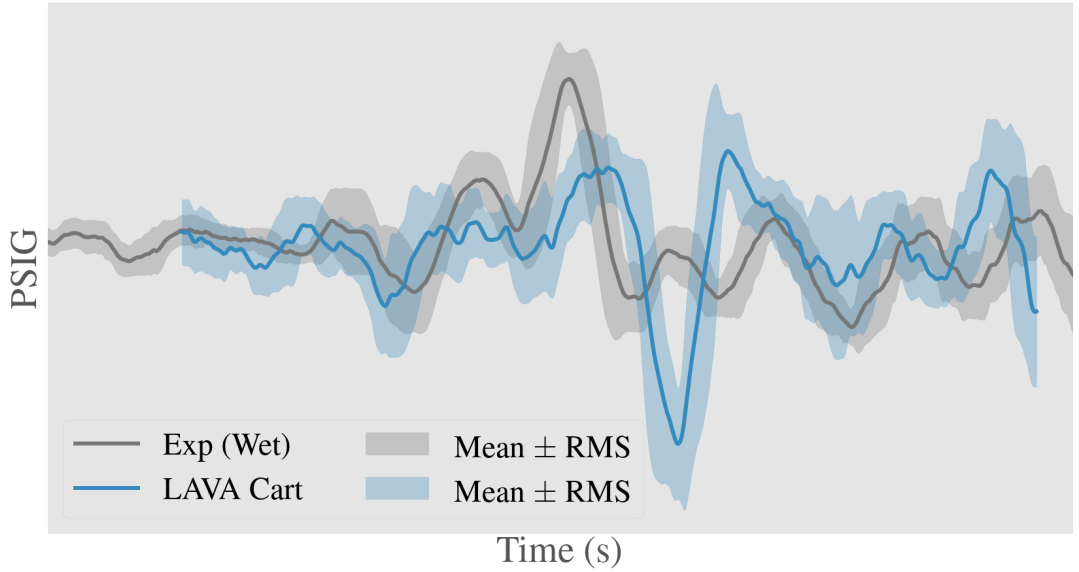

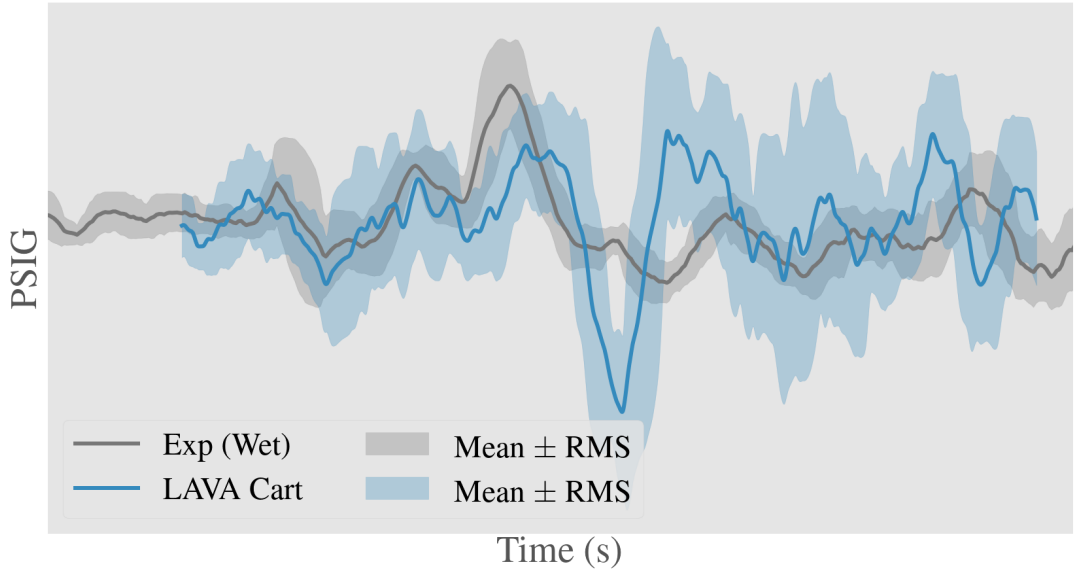

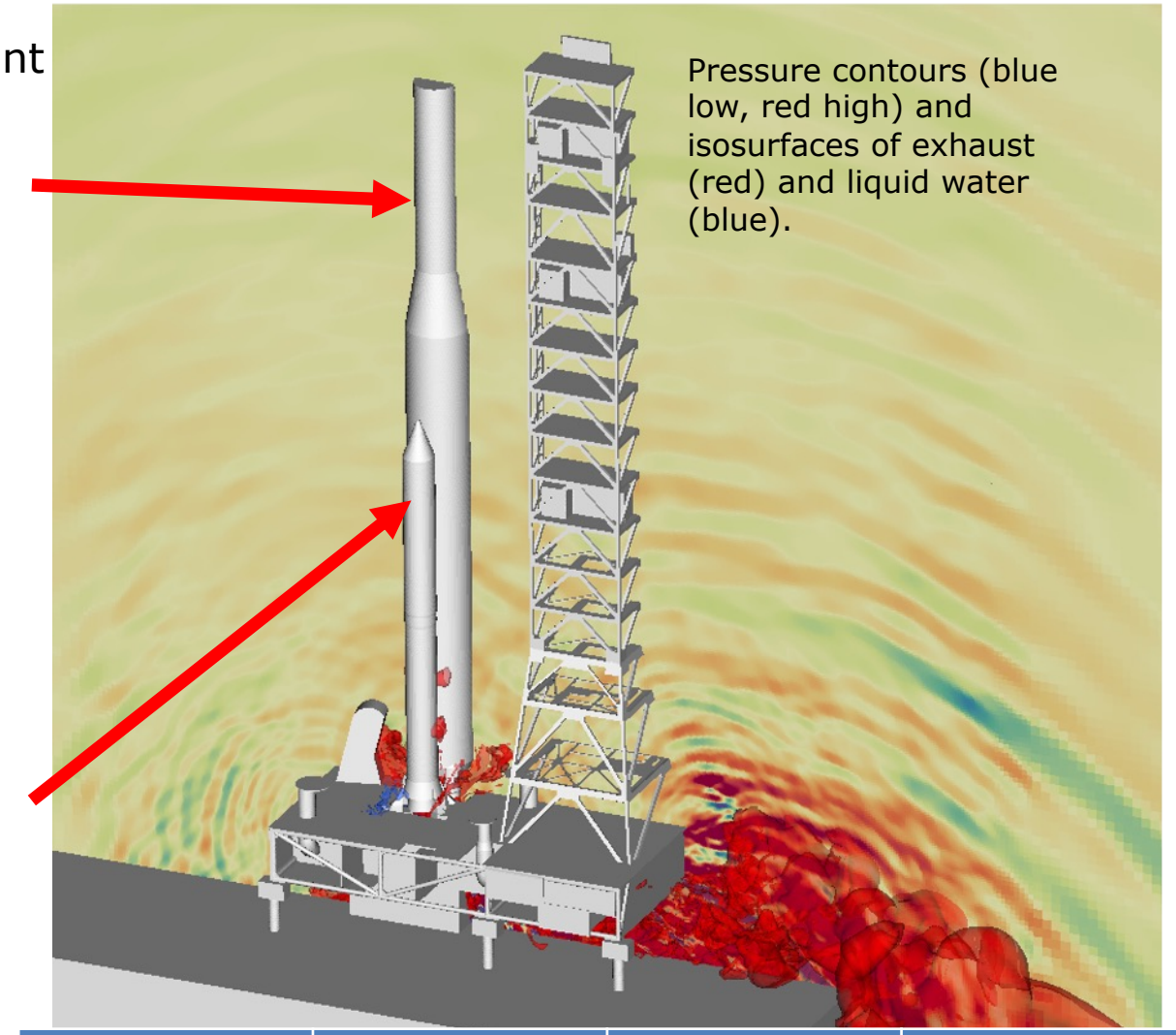

No. Cells	No. Cores	Model	Runtime
455M	8000	Skylake	~6.5 weeks

Scale Model Acoustic Test (SMAT): Wet Simulations with LAVA

- Slight under prediction in mean IOP wave
- Larger RMS in simulation
- Relatively good agreement

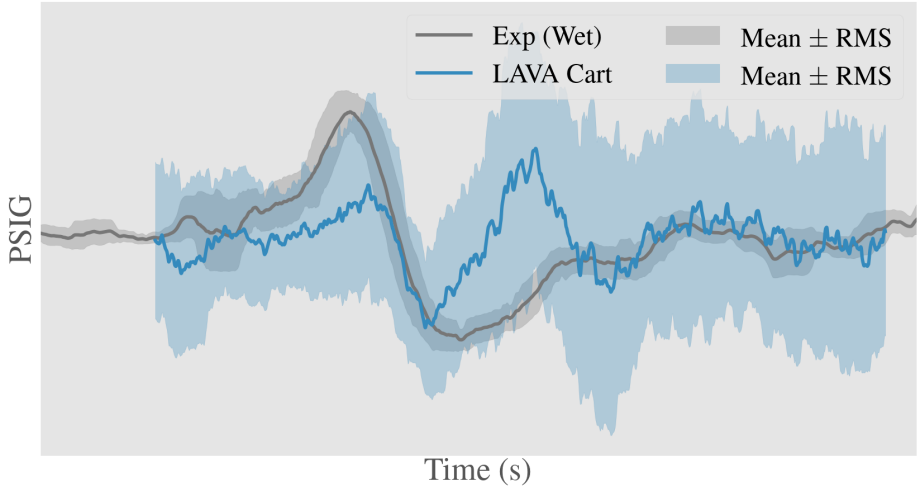

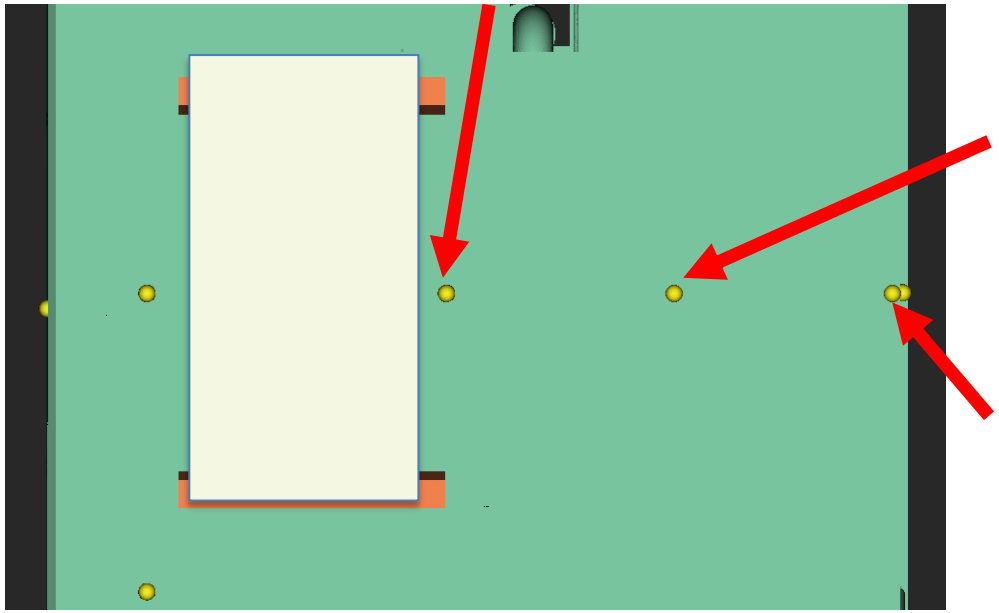

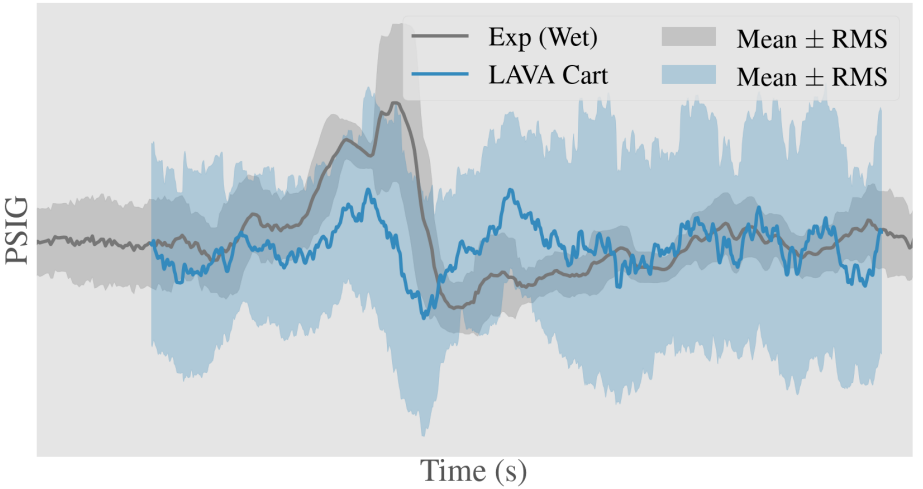

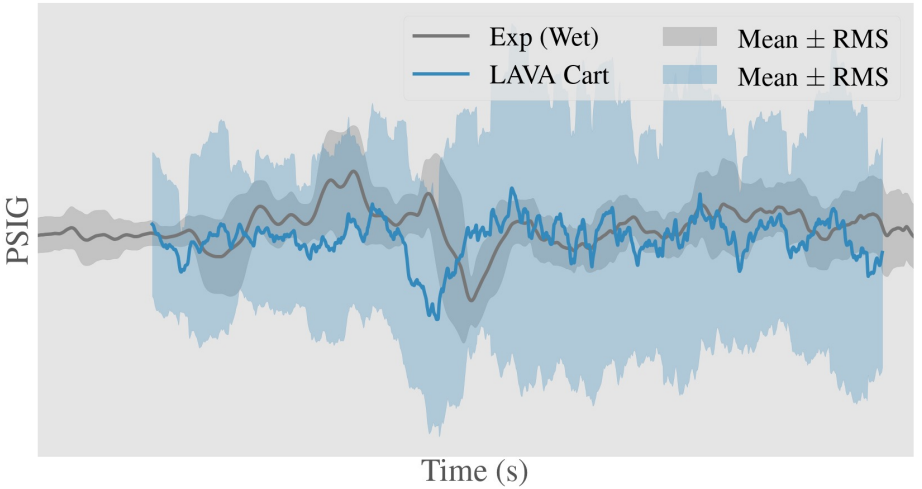

Artemis and the Space Launch System

- Future missions of NASA's Artemis program will utilize new launch vehicle configurations like the Space Launch System (SLS) to deliver assets to lunar orbit.

- More powerful launch vehicles means greater acoustic loads on the vehicle and the launch structure like the mobile launch pad

SLS rollout to LC-39B. Twitter @ulalaunch

Space Launch System (SLS) at LC-39B: Multiphase Simulations with LAVA (2021)

Volume rendering of exhaust and liquid water mass fractions.
For the liquid water, dark blue is high and light blue is low.
The exhaust plume mass fraction is colored so that high is yellow and low is purple. Geometry clipped to show flow features.

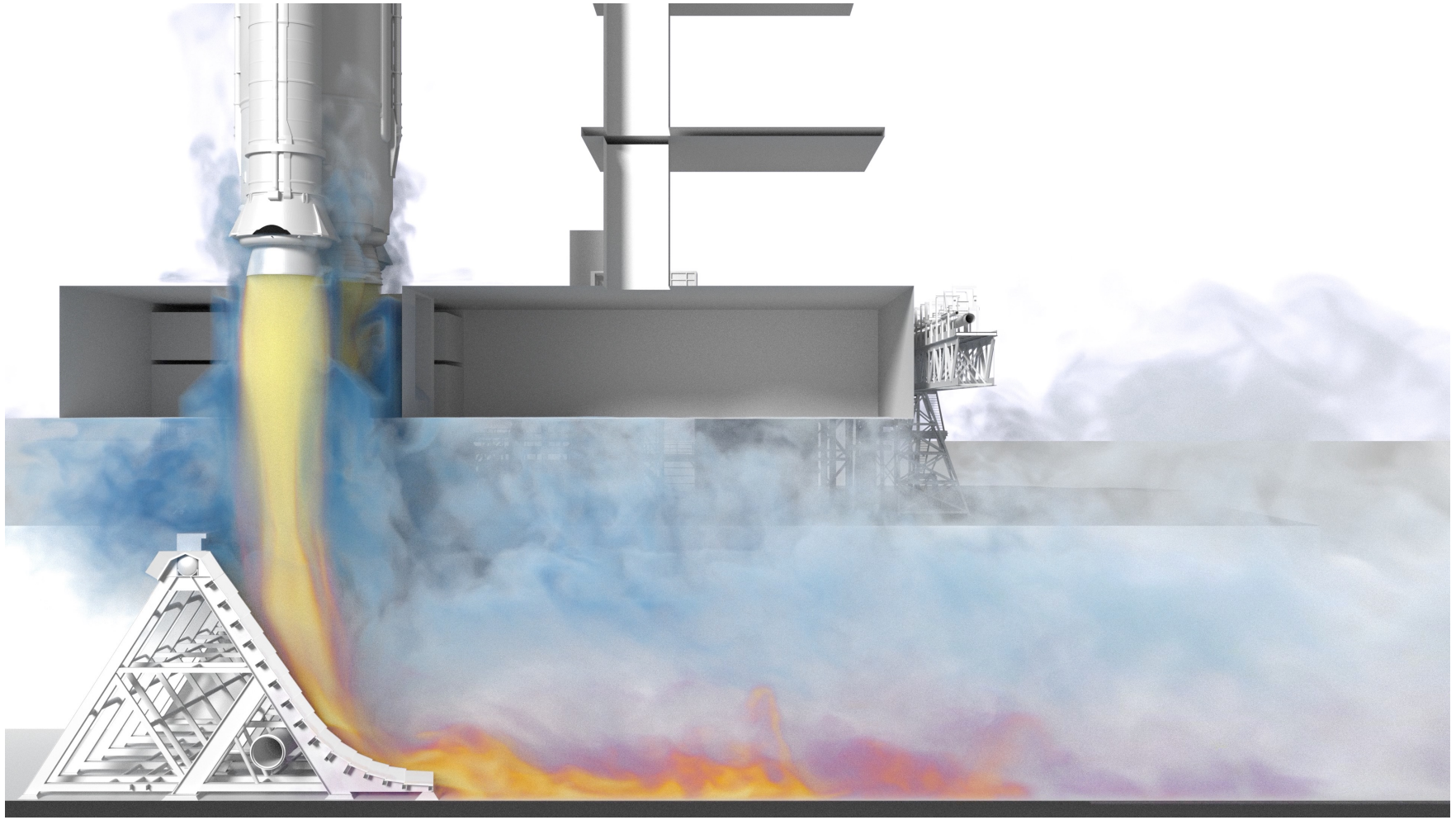

Space Launch System (SLS) at LC-39B: Multiphase Simulations with LAVA (2021)

Volume rendering of exhaust and liquid water mass fractions.
For the liquid water, dark blue is high and light blue is low.
The exhaust plume mass fraction is colored so that high is yellow and low is purple. Geometry clipped to show flow features.

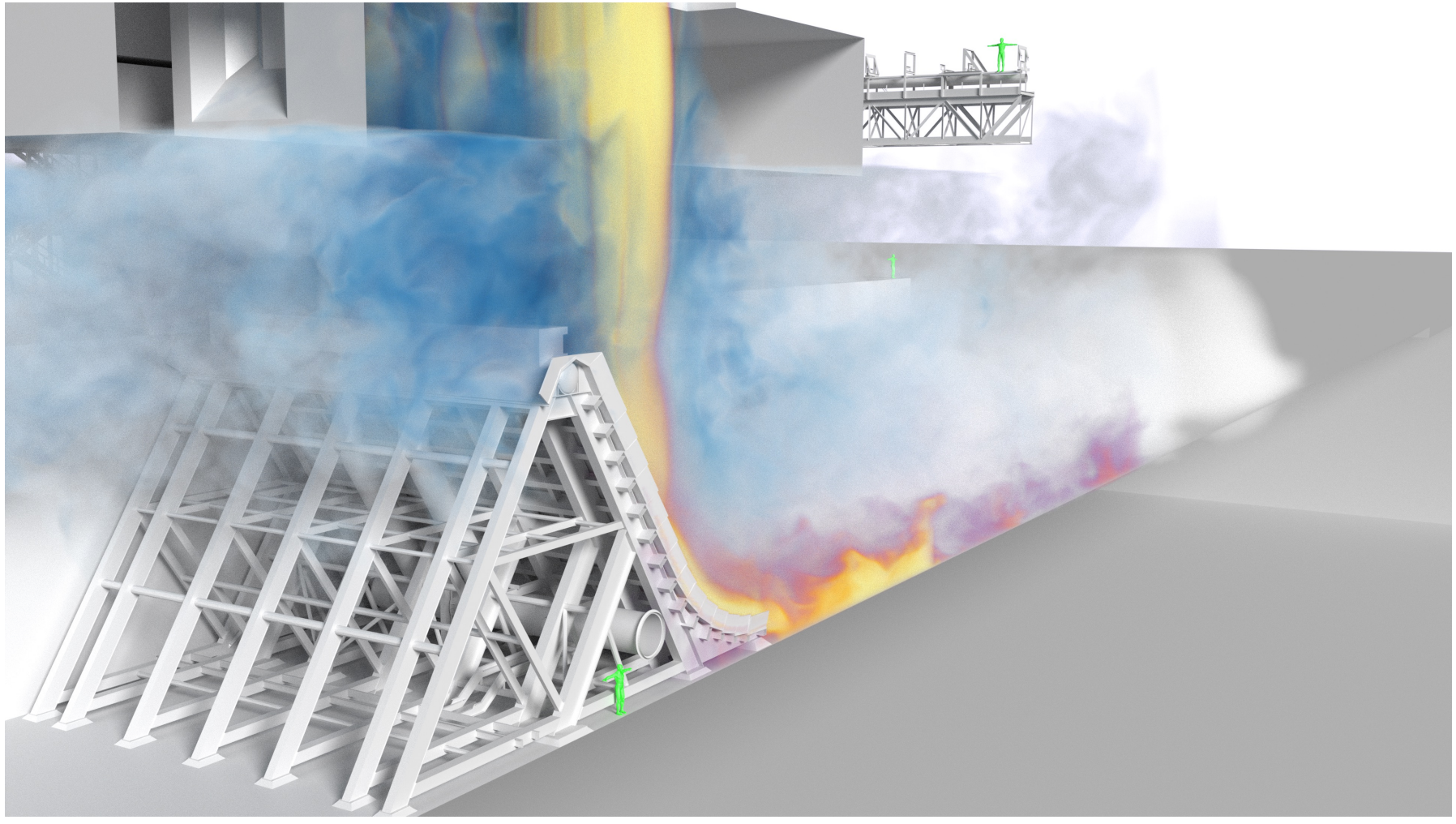

Space Launch System (SLS) at LC-39B: Multiphase Simulations with LAVA

- Pressure signal for wet case has been damped and attenuated compared to dry results
- Wet simulations show benefit of water-based IOP/SS system

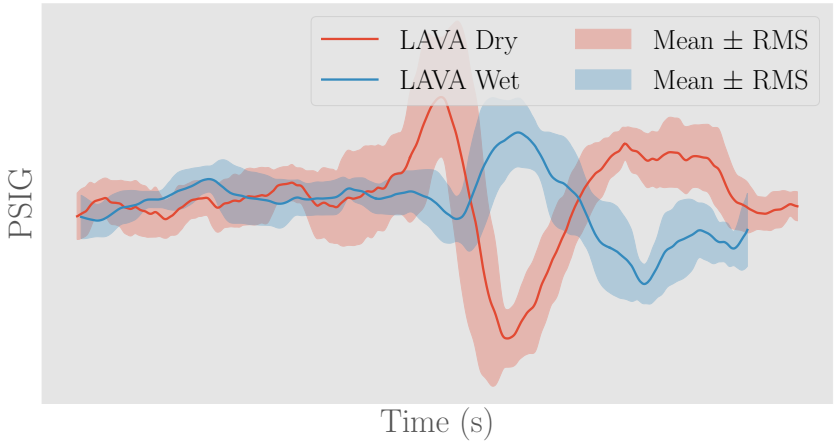

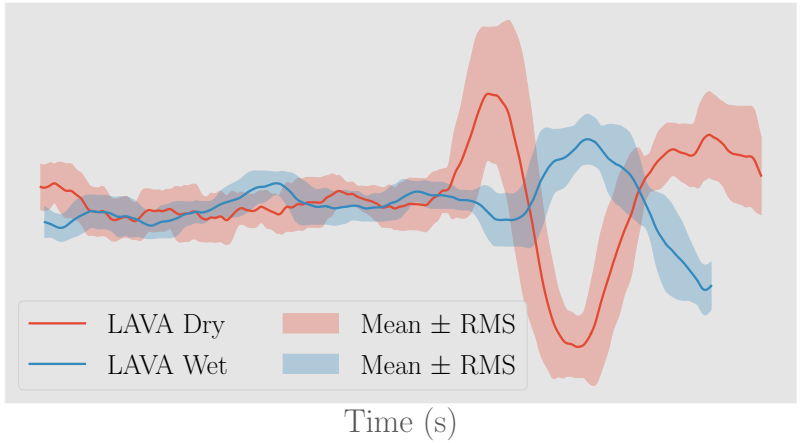

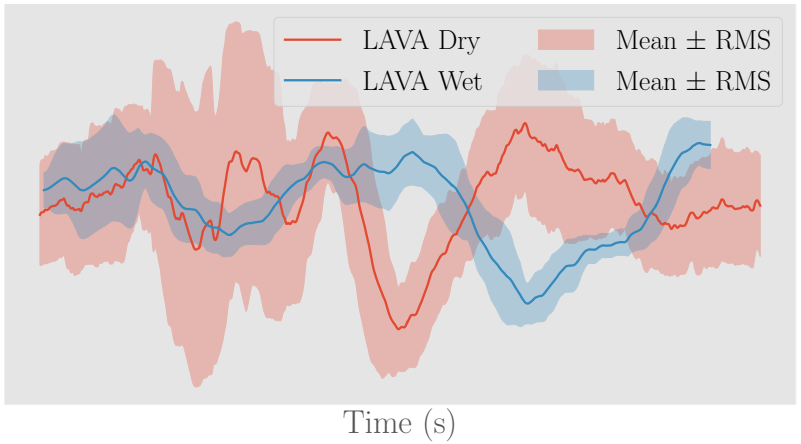

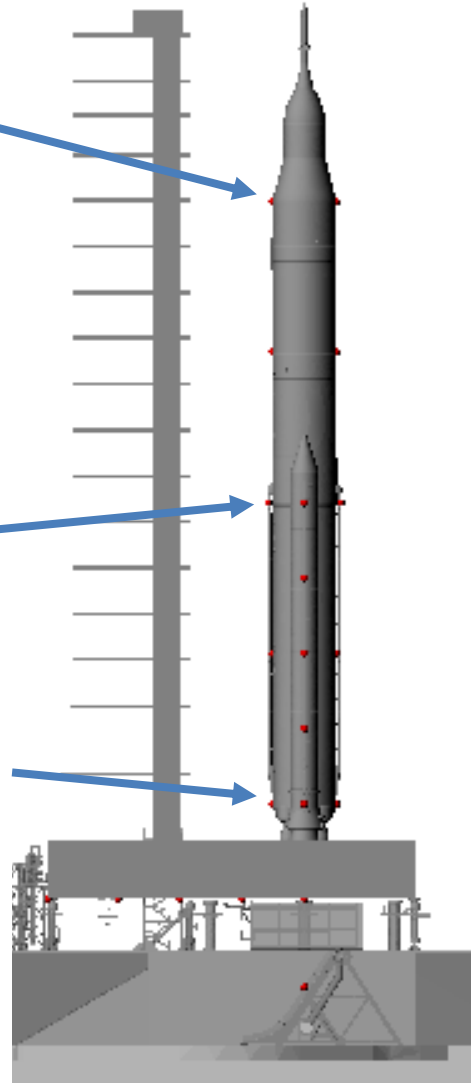

Space Launch System (SLS) at LC-39B: Multiphase Simulations with LAVA

Maximum gauge pressure felt on the underside of Mobile Launcher during the ignition of the SLS engines.

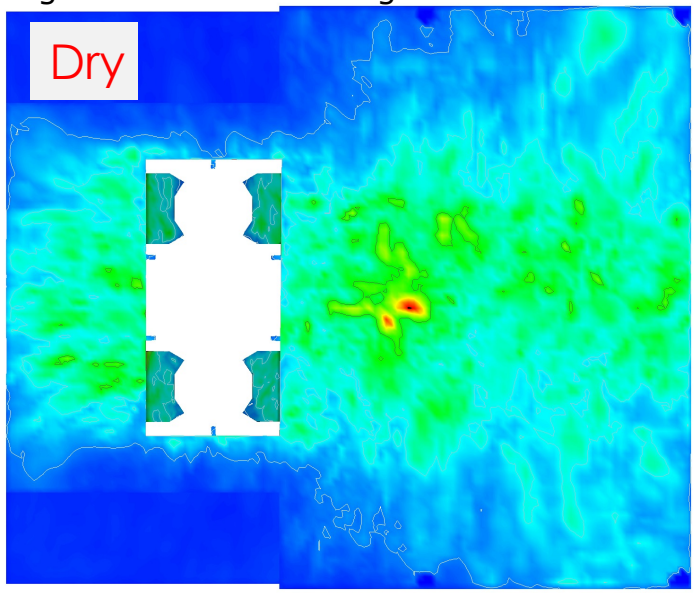

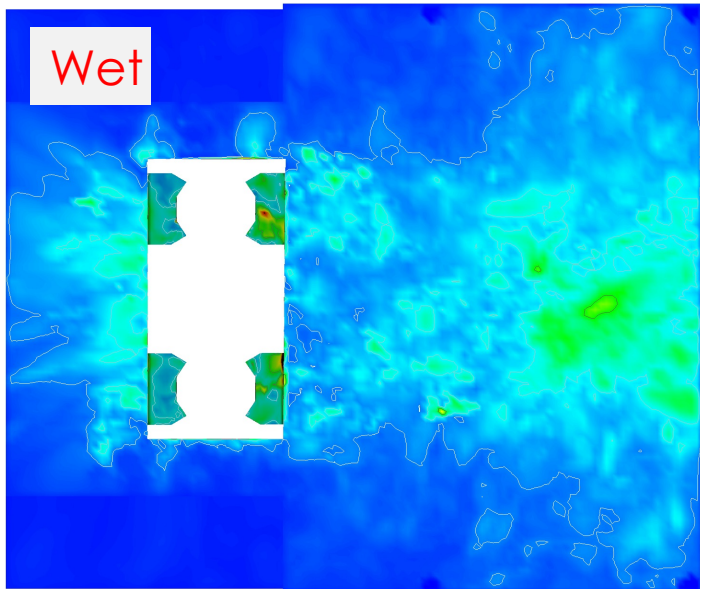

Comparison of ignition overpressure wave for dry and wet case at two sensor locations on the vehicle.

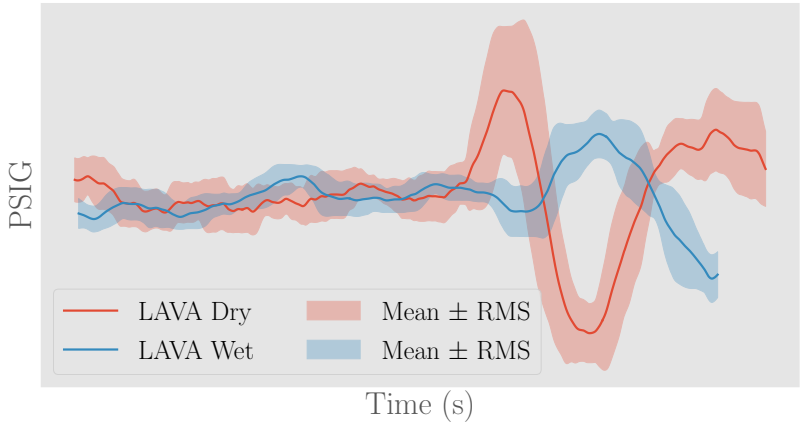

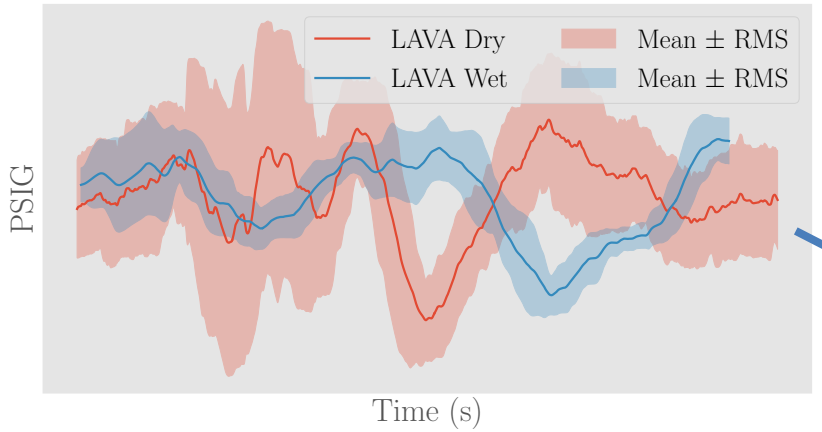

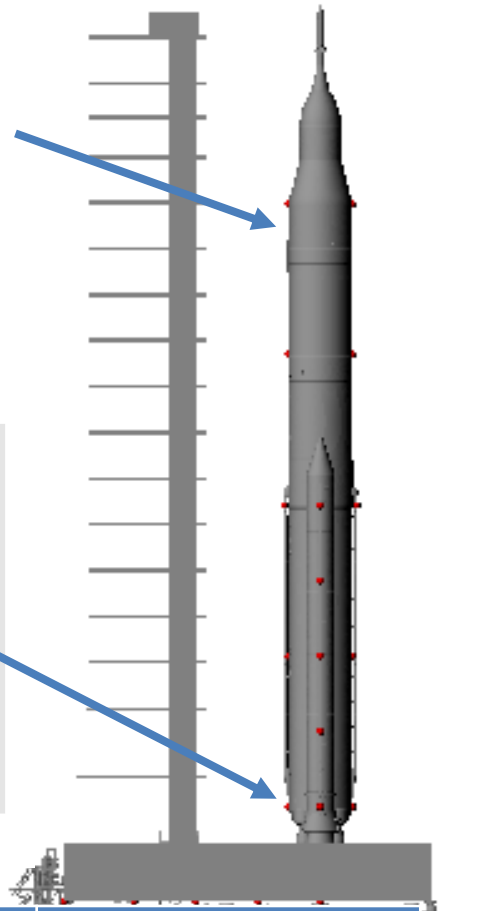

No. Cells	No. Cores	Model	Runtime
455M	8000	Skylake	~6.5 weeks

Summary

- Presented historical development of launch environment prediction capabilities at Ames/NAS
  - Shuttle era calculations with simplified geometries (2008)
  - LAVA development and validation for Space Shuttle (STS-135) launch environment simulations (2012)
  - Engineering design support for KSC Exploration Ground Systems:
    - Application of LAVA solver to dry SLS launch environment (2014)
    - Dry LAVA simulations give conservative estimates to assist main flame deflector redesign for SLS at LC-39B (2018)
- Developed a high-order, robust multiphase simulation capability in LAVA
  - Successful validation for SpaceX Falcon Heavy flight and engineering design analysis for LC-39A at NASA KSC
  - Successful validation for Scale Model Acoustic Test (SMAT) for dry and wet simulations
  - Validated procedure applied to upcoming **Artemis I** launch environment to demonstrate reduced loads on mobile launcher and SLS vehicle due to IOP/SS system

Outlook

- Recent refactoring of LAVA Cartesian code gives a >2x speedup. 6.5 weeks simulation time will be reduced to ~3 weeks

- Further validation efforts following **Artemis I** flight

Acknowledgments

- Project partially funded by NASA Exploration Ground Systems (EGS), NASA Launch Service Program (LSP), and NASA Engineering Safety Center (NESC). Special thanks to EGS for initiating the development of the multiphase capability
- Computations were performed at NASA Advanced Supercomputing (NAS) facilities at NASA Ames Research Center
- Thanks to
  - Bruce Vu (retired), Craig Fortier, and Nancy Zeitlin of NASA KSC for their collaborative efforts
  - Brandon Marsell of KSC LSP for providing information and support needed for simulations
  - Eric Beaser of SpaceX for providing information for Falcon Heavy simulations and feedback
  - Dave Schuster of NASA's NESC for valuable discussions and suggestions
  - James Jensen, Francois Cadieux, Emre Sozer, Jeff Housman, and other LAVA group members for helpful discussions and simulation preparations
  - Tim Sandstrom for visualizations

Backup Slides

Quasi-conservative Form for Equations of Motion

- Rewrite system of equations in quasi-conservative form

$$\partial_t \mathbf{W} + \partial_x \mathbf{F}(\mathbf{W}) + \mathbf{\Sigma}(\mathbf{W}, \nabla \mathbf{W}) = 0$$

with

$$\mathbf{F}(\mathbf{W}) = \begin{pmatrix} \alpha_1 \rho_1 u \\ \alpha_2 \rho_2 u \\ \rho u^2 + p \\ (E+p)u \\ 0 \end{pmatrix} \qquad \mathbf{\Sigma}(\mathbf{W}, \nabla \mathbf{W}) = \begin{pmatrix} 0 \\ 0 \\ 0 \\ 0 \\ u \partial_x \alpha_1 \end{pmatrix}$$

- System of equations is quasi-conservative. Last equation not conservative, but only contributes a linearly degenerate contact wave, doesn't change the genuinely nonlinear waves

- To derive a numerical approximation, we consider a 1D generalized Riemann problem

HLLC Approximate Riemann Solver for Five Equation Model

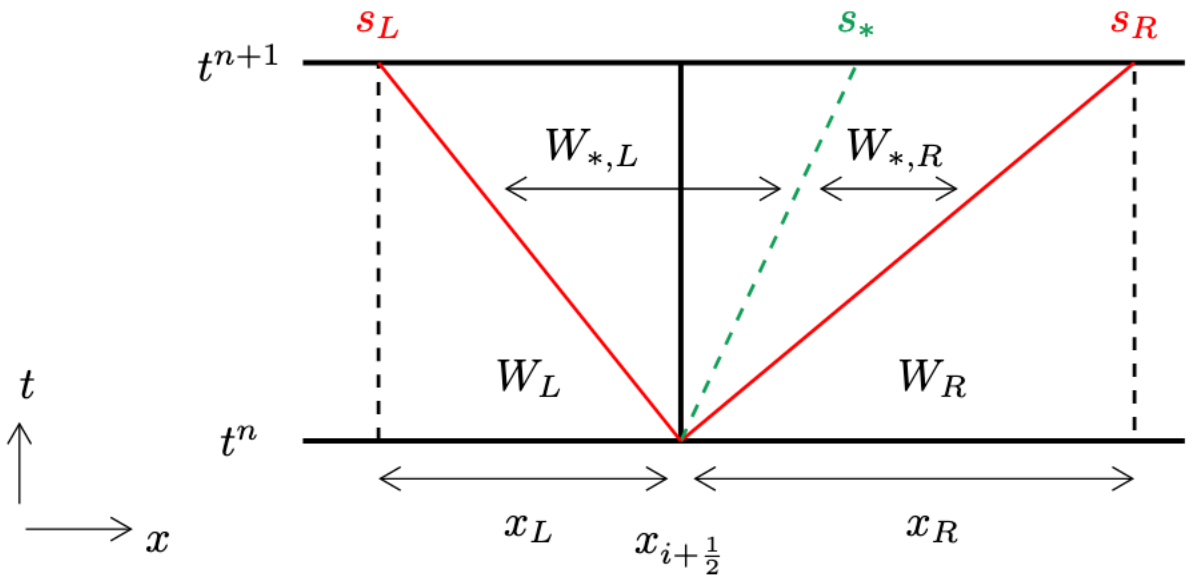

$$\mathbf{W}^{\mathrm{HLLC}} = \begin{cases} \mathbf{W}_L, & \text{if } s_L > 0, \\ \mathbf{W}_{*,L}, & \text{if } s_L \leq 0 < s_*, \\ \mathbf{W}_{*,R}, & \text{if } s_* \leq 0 \leq s_R, \\ \mathbf{W}_R, & \text{if } s_R < 0, \end{cases}$$

Approximate hyperbolic structure with three waves: two acoustic waves, one contact wave

$$\mathbf{W}_{*,K} = \begin{pmatrix} \chi_{*,K} \left(\alpha_1 \rho_1\right)_K \\ \chi_{*,K} \left(\alpha_2 \rho_2\right)_K \\ \chi_{*,K} \rho_K s_* \\ \chi_{*,K} \rho_K v_K \\ \chi_{*,K} \left[E_K + (s_* - u_K) \left(\rho_K s_* + \frac{p_K}{s_K - u_K} \right) \right] \\ \alpha_{1,K} \end{pmatrix}$$

No jump in volume fraction for left and right waves

$$\chi_{*K} = \frac{s_K - u_K}{s_K - s_*}.$$

Deriving Approximate Fluxes with HLLC Solver

- To derive a numerical flux, we rewrite system of equations in more convenient flux-source form

$$\partial_t \mathbf{W} + \partial_x \mathbf{G}(\mathbf{W}) = \mathbf{S}(\mathbf{W}, \nabla \mathbf{W})$$

with

$$\mathbf{G}(\mathbf{W}) = \begin{pmatrix} \alpha_1 \rho_1 u \\ \alpha_2 \rho_2 u \\ \rho u^2 + p \\ (E+p)u \\ \alpha_1 u \end{pmatrix} \qquad S(\mathbf{W}, \nabla \mathbf{W}) = \begin{pmatrix} 0 \\ 0 \\ 0 \\ 0 \\ \alpha_1 \partial_x u \end{pmatrix}$$

$$\mathbf{G}(\mathbf{W}) = \mathbf{F}(\mathbf{W}) + \begin{pmatrix} 0 & 0 & 0 & 0 & f_\alpha \end{pmatrix}^T$$

- First-order fully discretized form of equations

$$\frac{\mathbf{W}_i^{n+1} - \mathbf{W}_i^n}{\Delta t} + \frac{\hat{\mathbf{G}}_{i+\frac{1}{2}} - \hat{\mathbf{G}}_{i-\frac{1}{2}}}{\Delta x} = \hat{\mathbf{S}}_i \qquad \hat{\mathbf{S}}_i = \begin{pmatrix} 0 \\ 0 \\ 0 \\ 0 \\ \alpha_{1i}^n \left(\frac{\hat{u}_{i+\frac{1}{2}} - \hat{u}_{i-\frac{1}{2}}}{\Delta x} \right) \end{pmatrix}$$

Deriving Approximate Fluxes with HLLC Solver

- Using previous HLLC approximate Riemann solver, we define the numerical flux

$$\hat{\mathbf{G}}_{i+\frac{1}{2}} = F^{\mathrm{HLLC}}_{i+\frac{1}{2}} + \begin{pmatrix} 0 & 0 & 0 & 0 & f^{\mathrm{HLLC}}_{\alpha,i+\frac{1}{2}} \end{pmatrix}$$

- Nonconservative volume fraction equation makes of use interface velocity from HLLC star state

$$\hat{\mathbf{G}}^{\pm}_{i\mp\frac{1}{2}} = \hat{\mathbf{G}}_{i\mp\frac{1}{2}} - \alpha_{1i} \begin{pmatrix} 0 & 0 & 0 & 0 & \hat{u}_{i\mp\frac{1}{2}} \end{pmatrix}^T$$

$$\mathbf{W}^{n+1}_i = \mathbf{W}^n_i - \frac{\Delta t}{\Delta x}\left(\hat{\mathbf{G}}^{-}_{i+\frac{1}{2}} - \hat{\mathbf{G}}^{+}_{i-\frac{1}{2}}\right)$$

Lemma 2: The HLLC approximate Riemann solver produces a star state in G if left and right states are also in G

Finite Volume Interpretation for Update

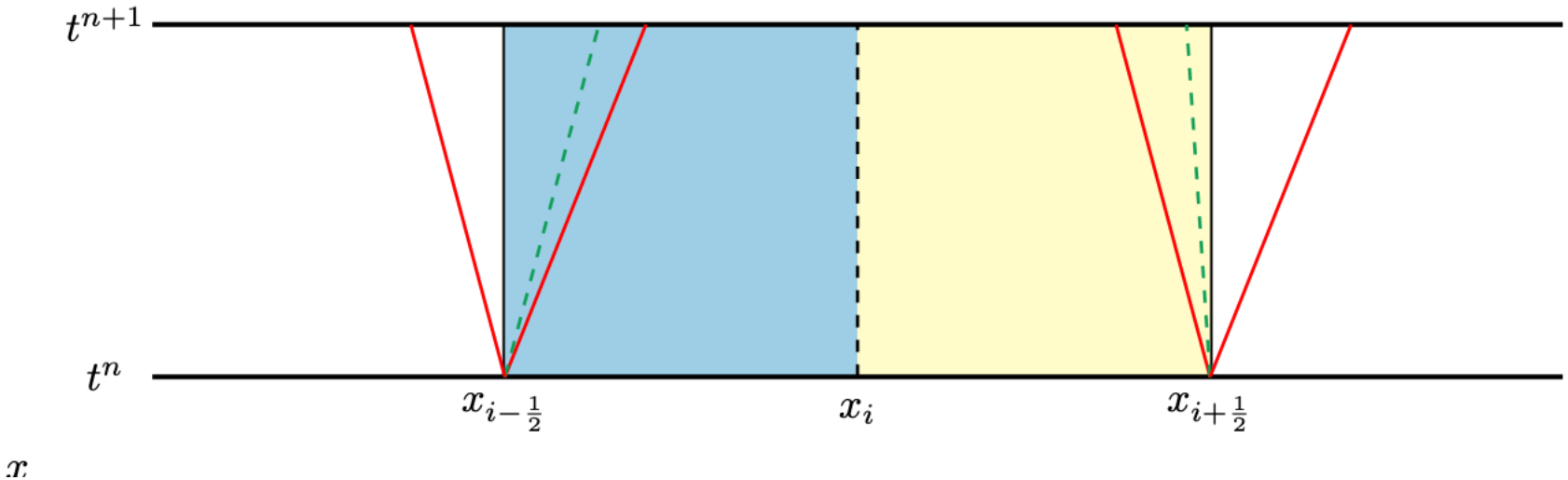

First-order update formula given by

$$\mathbf{W}_i^{n+1} = \mathbf{W}_i^n - \frac{\Delta t}{\Delta x}\left(\hat{\mathbf{G}}^-_{i+\frac{1}{2}} - \hat{\mathbf{G}}^+_{i-\frac{1}{2}}\right)$$

From finite volume approach we can interpret the cell averages as follows

$$\frac{1}{\Delta x}\int_{x_{i-\frac{1}{2}}}^{x_i} R\left(\frac{x - x_{i-\frac{1}{2}}}{\Delta t}, \mathbf{W}_{i-1}^n, \mathbf{W}_i^n\right) \mathrm{d}x = \frac{1}{2}\left[\mathbf{W}_i^n - 2\frac{\Delta t}{\Delta x}\left(\mathbf{F}_i - \hat{\mathbf{G}}^+_{i-\frac{1}{2}}\right)\right]$$

$$\frac{1}{\Delta x}\int_{x_i}^{x_{i+\frac{1}{2}}} R\left(\frac{x - x_{i+\frac{1}{2}}}{\Delta t}, \mathbf{W}_i^n, \mathbf{W}_{i+1}^n\right) \mathrm{d}x = \frac{1}{2}\left[\mathbf{W}_i^n - 2\frac{\Delta t}{\Delta x}\left(\hat{\mathbf{G}}^-_{i+\frac{1}{2}} - \mathbf{F}_i\right)\right]$$

First-Order Scheme is Positivity Preserving

Lemma 1: G is a convex set i.e.; *G is closed under convex combinations of elements in G*

Lemma 2: The HLLC approximate Riemann solver produces an admissible state if left and right states are also admissible

Theorem: Under suitable CFL condition, the first-order scheme using the HLLC approximate Riemann solver produces an updated state that is in G.

Sketch of proof:
Under suitable CFL restriction, neighboring Riemann problems do not interact, and first-order finite volume update can be written as the convex combination,

$$\mathbf{W}_i^{n+1} = \frac{1}{\Delta x}\int_{x_{i-\frac{1}{2}}}^{x_i} R\left(\frac{x - x_{i-\frac{1}{2}}}{\Delta t}, \mathbf{W}_{i-1}^n, \mathbf{W}_i^n\right)\,\mathrm{d}x + \frac{1}{\Delta x}\int_{x_i}^{x_{i+\frac{1}{2}}} R\left(\frac{x - x_{i+\frac{1}{2}}}{\Delta t}, \mathbf{W}_i^n, \mathbf{W}_{i+1}^n\right)\,\mathrm{d}x$$

By Lemma 2, self-similar solution given by approximate Riemann solver $R\left(\frac{x}{t}, W_L, W_R\right)$ is in G. Further, since Lemma 1 says G is convex, Jensen's inequality for integral equations implies the updated state is also in G.

Achieving High-Order Accuracy

Write system in a semi-discretized form

$$\frac{\mathrm{d}}{\mathrm{d}t}u_i = -\left(\frac{\partial \mathbf{F}}{\partial x}\right)_i$$

Hybrid midpoint-node differencing

$$\left(\frac{\partial \mathbf{F}}{\partial x}\right)_i = \frac{\alpha}{\Delta x}\left(\hat{\mathbf{F}}_{i+\frac{1}{2}} - \hat{\mathbf{F}}_{i-\frac{1}{2}}\right) + \frac{192-175\alpha}{256\Delta x}\left(\mathbf{F}_{i+1} - \mathbf{F}_{i-1}\right) + \frac{35\alpha - 48}{320\Delta x}\left(\mathbf{F}_{i+2} - \mathbf{F}_{i-2}\right) + \frac{64-45\alpha}{3840\Delta x}\left(\mathbf{F}_{i+3} - \mathbf{F}_{i-3}\right)$$

Can be written in a flux reconstruction form, conservative except for volume fraction transport equation

$$\left(\frac{\partial \mathbf{F}}{\partial x}\right)_i = \frac{\tilde{\mathbf{F}}_{i+\frac{1}{2}} - \tilde{\mathbf{F}}_{i-\frac{1}{2}}}{\Delta x}$$

Reconstructed flux requires high-order numerical flux and velocities at the cell j faces

X. Deng, M. Mao, Y. Jiang, H. Liu,. "New high-order hybrid cell-edge and cell-node weighted compact nonlinear schemes." 2011.

A. Subramaniam, M. L. Wong, and S. K. Lele. "A high-order weighted compact high resolution scheme with boundary closures for compressible turbulent flows with shocks." Journal of Computational Physics, 2019

Interpolation and Flux Limiting Procedure

- High-order accurate velocity and numerical fluxes at cell faces constructed with robust WENO interpolation

- WENO interpolation is robust but not strictly positivity preserving. HLLC solver must have admissible states as input. If the interpolated state is not admissible, we compute a limited state e.g., for sound speed squared we compute

$$\left(1-\theta_{i+\frac{1}{2}}\right)\rho c^2\left(\mathbf{W}_i\right)+\theta_{i+\frac{1}{2}}\rho c^2\left(\tilde{\mathbf{W}}_{i+\frac{1}{2}}\right)=\epsilon$$

$$\mathbf{W}^*_{i+\frac{1}{2}}=\left(1-\theta_{i+\frac{1}{2}}\right)\mathbf{W}_i+\theta_{i+\frac{1}{2}}\tilde{\mathbf{W}}_{i+\frac{1}{2}}$$

- Similar limiting calculation done for partial densities and volume fractions to ensure boundedness (omitted here)

- The high-order reconstructed flux may also fail to give an admissible update, so we also limit the reconstructed flux with the first-order flux to preserve positivity of volume fractions, partial densities, and sound speed squared.

Novel Robust Method for Multiphase Simulations

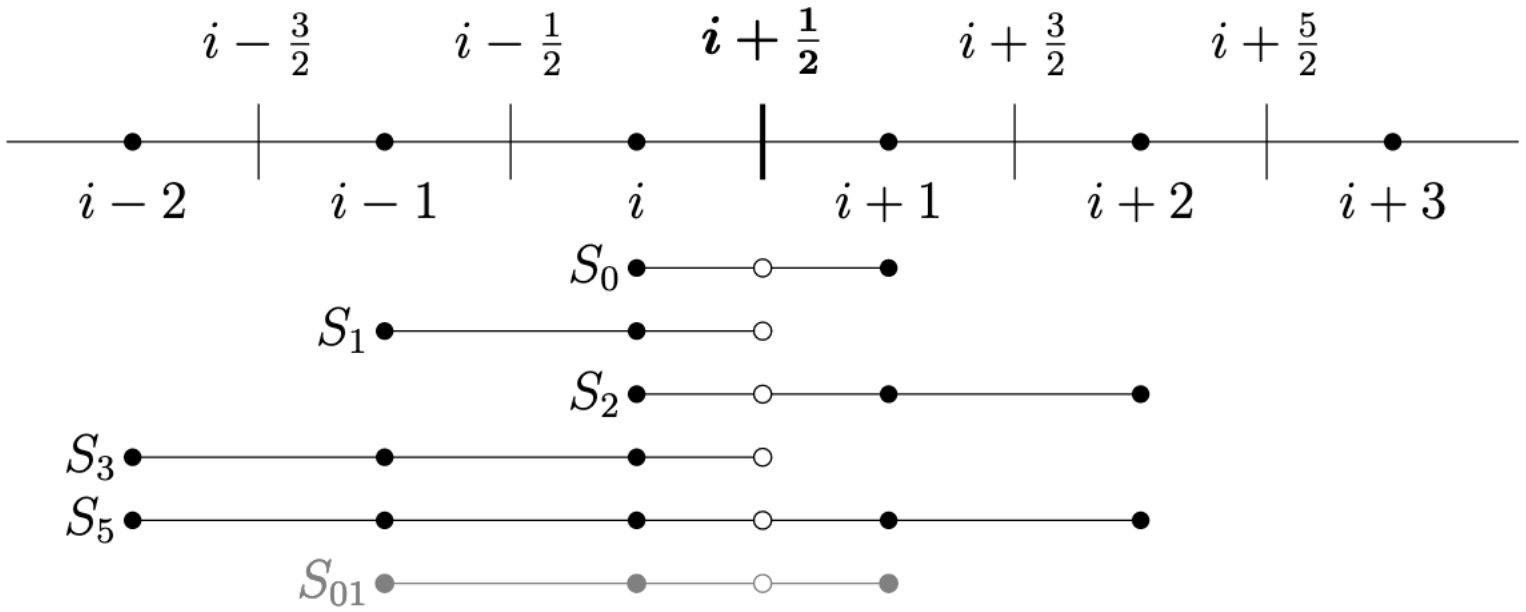

X. Deng. "New high-order hybrid cell-edge and cell-node weighted compact nonlinear schemes." 2011.

Novel Robust Method for Multiphase Simulations

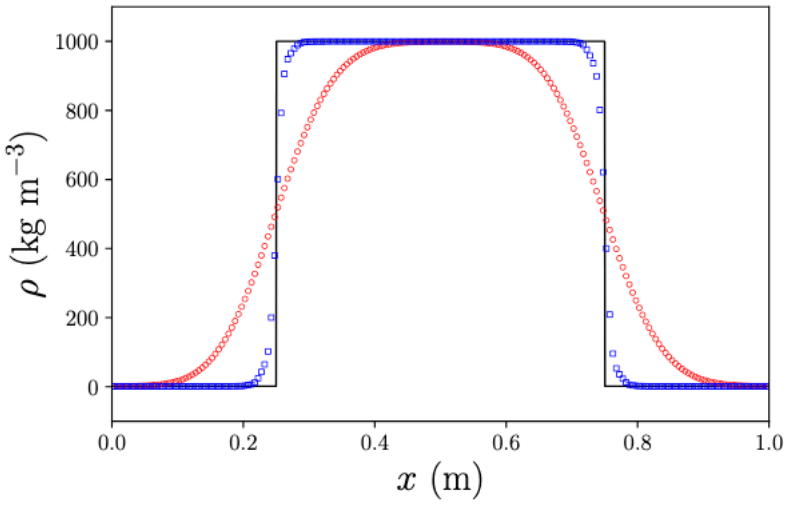

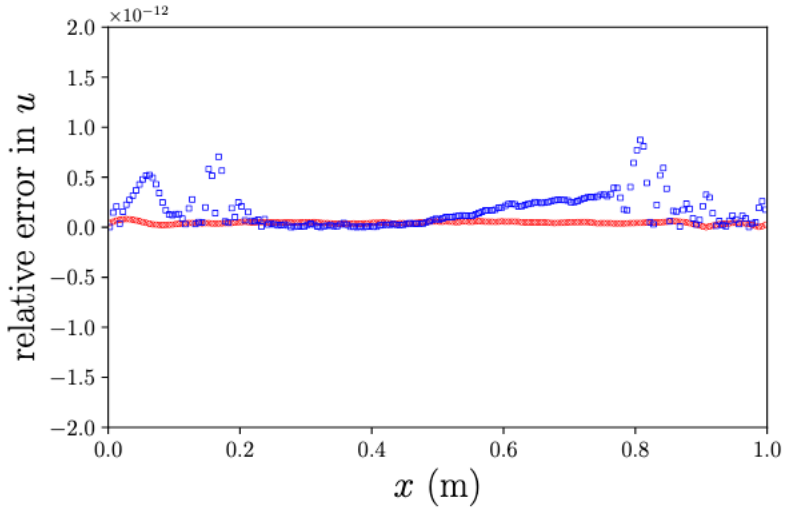

(a) Velocity

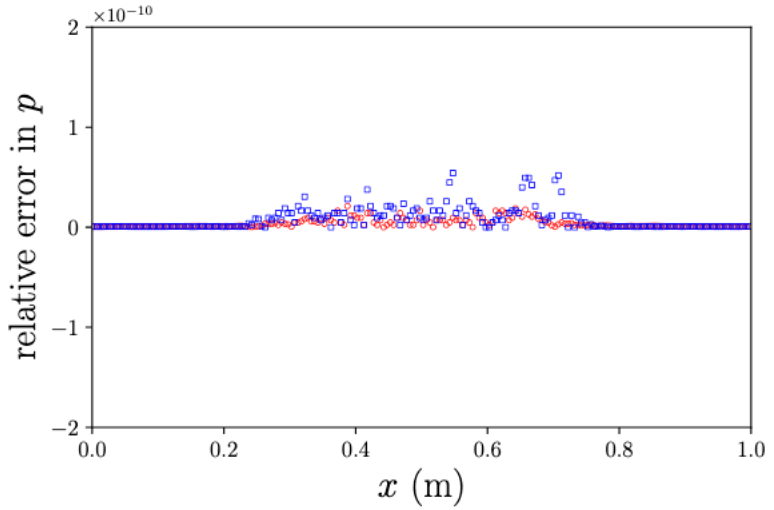

(b) Pressure